3 Experimental Results

3.1 Introduction

Experimental results are presented in this chapter. The presentation is first focused on the observations of the behavior of full and small scale specimens during the tests. Results of small scale series #1 specimens which gave the general indication of the effect of edge web restraining, shear span, slab thickness, end details and slenderness are presented next. Then results of small scale series #2 and full scale tests are presented and compared. Loads at a *span*/360 deflection limit and a comparison with the design load is presented. Discussions on failure mode to indicate the ductility of the specimens are also presented. Lastly, strain gage readings from full scale tests are presented to provide experimental evidence as to whether or not the steel had yielded when the slab failed.

Through out the discussions the specimens are identified either by ID labels or by the test numbers as given in Table 2.2, 2.3 and 2.4 for full scale, small scale series #1 and small scale series #2, respectively. When comparison between the full scale and small scale tests are made, a letter *s* or *f* was added to the specimen ID. Because two tests were performed for each configuration, a capital letter *A* or *B* is used for the two specimens. It should be noted also that the term *compact slab* is used to refer to short and thick specimens, particularly those 6.5 and 7 in. thick with span length 7 and 8 ft or shorter. On

the other hand, the term *slender slab* refers to the 4 and 5 in. thick specimens with spans ranging from 9 to 14 ft.

To facilitate comparison between results, all loads are presented as equivalent uniform loads. The calculation was made by equating the maximum moments in the test specimen to the maximum moment of a uniformly loaded simply supported specimen. For full scale specimens and small scale specimens in series #2, equivalent uniform loads were calculated based on clear span lengths measured between the interior edges of support beam flanges. For series #1, the length was measured from centers of supports. Loading beam and spreader beam weight were added to the load cell reading. The slab and deck self weight was neglected in all results because their effect was small and negligible in the composite action. The deck deflection due to fresh concrete was also neglected in the composite slab measurement.

3.2 Non composite deck

The measured and theoretical deflections of the steel decks under fresh concrete for full scale specimens are shown in Table 3.1. The theoretical calculation was made according to the linear elastic flexural deflection equation as given by $\Delta = \frac{5wL^4}{384EI_s}$, where w = weight of deck and fresh concrete taken as 150 pcf, L = clear span length, E = modulus of elasticity, taken as 29500 ksi, and I_s = moment of inertia of steel deck. The measured-to-calculated deflection ratios are generally in the range of 1.1-1.4. The difference was due to the use of clear span length which theoretically increased the deck stiffness and this may not represent the stiffness of the actual decks that were fixed to the support beam by puddle welds at 1 ft on centers. Span B of 3VL16-8-7.5 was an exception, as the difference was

exceptionally large. An instrumentation error or malfunction was suspected to have occurred but was not confirmed.

Table 3.1 Measured and calculated deflections due to fresh concrete for non-composite deck of full scale specimens

Specimen	Span	Measured deflection, Δ_t at mid span (in.)	Calculated deflection, Δ at mid span (in.)	Δ_t/Δ
3VL20-8-7.5	Span A	0.209	0.181	1.15
	Span B	0.238		1.31
3VL20-11-5	Span A	0.541	0.425	1.27
	Span B	0.539		1.27
3VL18-8-7.5	Span A	0.181	0.137	1.32
	Span B	0.187		1.36
3VL18-13-5	Span A	0.822	0.657	1.25
	Span B	0.808		1.23
3VL16-8-7.5	Span A	0.131	0.110	1.19
	Span B	0.27		2.46
3VL16-14-5	Span A	0.797	0.722	1.10
	Span B	0.811		1.12
2VL20-7-6.5	Span A	0.268	0.208	1.29
	Span B	0.26		1.25
2VL20-9-4	Span A	0.31	0.347	0.89
	Span B	0.433		1.25
2VL18-7-6.5	Span A	0.175	0.157	1.11
	Span B	0.181		1.15
2VL18-11-4	Span A	0.811	0.626	1.30
	Span B	0.787		1.26
2VL16-7-6.5	Span A	0.166	0.126	1.32
	Span B	0.161		1.28
2VL16-12-4	Span A	0.893	0.729	1.22
	Span B	0.834		1.14

3.3 Behavior results for full scale tests

The behavior of full scale specimens are discussed here in detail. For small scale specimens especially those in series #2, the behavior was identical to the full scale specimens and therefore will only be touched on briefly following this section.

Typical load-deflection and load-end slip curves for slender and compact slabs, as exhibited by 2VL20-9-4f-B (slender) and 2VL20-7-6.5f-B (compact), respectively are shown in Fig. 3.1. Note that end slip is given in the upper scale. Other test results might deviate somewhat from these curves, but the trend can be generalized to follow similar patterns for both small and full scale tests that failed in shear bond. Differences between the small and full scale results are discussed in the following section.

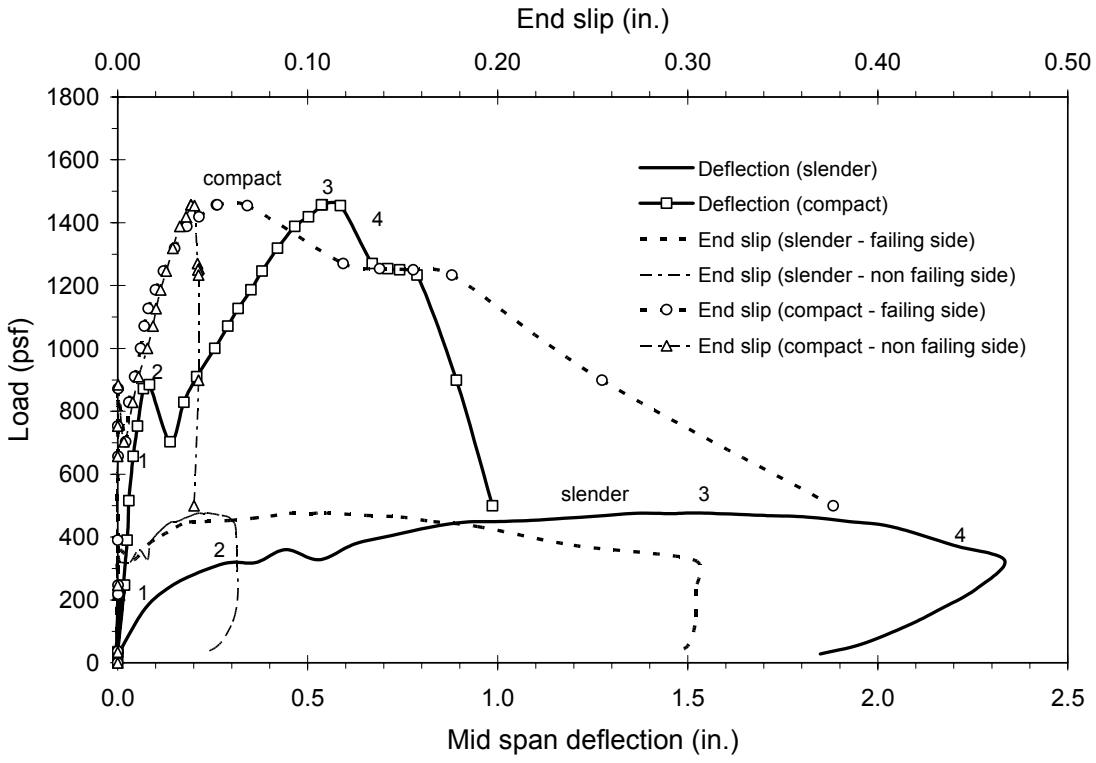

Fig. 3.1 Typical load-deflection and load-end slip relationship for slender and compact slabs.

Generally, for the full scale specimens, the concrete began to crack over the interior support in the early stages of loading. In some cases cracks were already visible before the load was applied. This implied that the continuity of the concrete without negative reinforcement was not effective in providing rotational stiffness at the interior support. In the beginning of loading, the slabs displacement responded linearly with the loads up to level 1 of Fig. 3.1, then flexural cracks began to develop near the line loads and in the constant moment region. Popping sounds were heard during this period indicating the breaking of chemical bond. As the loads increased between points 1 and 2, new cracks developed, existing ones enlarged and end slip initiated. Slender slabs developed a larger number of vertical cracks in the constant moment region than the compact ones.

At some point during the tests, which is qualitatively indicated by point 2, the pour stop welds at exterior ends failed and the slab end rotated and appeared to be bearing only on the interior flange edge of the support beam. The weld failure was usually accompanied by a loud sound and a significant reduction of slab stiffness. This failure is indicated in the graphs by reduction of applied load and significant increment of vertical deflection. Also at this point the end slip rate increased. On the interior support, the negative moment crack enlarged and the slab also appeared to rotate freely. However no sign of weld failure was observed at the interior support. Fig. 3.2(a) and (b) show typical end conditions of the slabs at failure while Fig. 3.3(a) shows a typical crack at critical section under or near line load as a result of shear bond failure along the shear span.

It was also observed that for the slabs that failed by shear bond, the top flange of the deck buckled at the critical section as shown in Fig. 3.3(b). The buckling of the flange occurred shortly after the ultimate load was attained. Typically, the buckling was

noticeable when the loads had reduced to point 4, after which the specimens lost composite action and the load resistance was completely attributable to steel deck alone. For compact slabs, the top flange buckling occurred more suddenly than the slender ones and in some cases, was accompanied by a loud sound and abrupt formation of a hinge. As the full scale experiments were used to substantiate the admissibility of the small scale test procedure developed in this research, their quantitative results will be presented together with the small scale result later in Sec. 3.6.

(a) **(b)**

Fig. 3.2 Typical end condition at failure
(a) Exterior support (b) Interior support

(a) **(b)**

Fig. 3.3 Concrete cracking and flange buckling
(a) Major crack due to slip failure. (b) Buckling of deck top flange

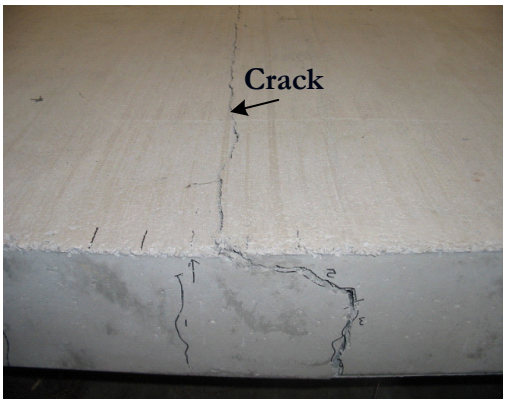

Fig. 3.4 Typical concrete cracking after failure

At final condition, the major crack grew up to the concrete top fiber resulting in the concrete being completely separated into two parts (Fig. 3.4). This crack behavior is observed in all compact slabs. In slender slabs the crack also grew up to the top fiber but the complete concrete separation was not obvious. None of the slabs had indication of concrete crushing.

3.4 Behavior results for small scale tests – series #1 and series #2

3.4.1 Small scale series #1

All specimens in series #1 failed by shear bond with significant slips recorded at the ends and major cracks occurring at the critical section below one of the two point loads. Small cracks due to bending were also observed in the constant moment region. No attempt was made to measure the vertical separation. However it was observed that the concrete and the decks were separated vertically as a result of concrete overriding as shown in Fig. 3.5. Specimens with fewer straps, namely Specimen #13 in series #1 exhibited larger vertical separation than those with more straps in the same series. Due to this observation, it was decided that the frequency of straps in series #2 be increased to 4 in. interval along

the entire length. Test A of specimens #20 where the concrete cover was 2 in. above deck top flange also cracked longitudinally along the shear span as shown in Fig. 3.6.

(a) (b)

Fig. 3.5 Vertical separation
(a) End of slab, (b) Side of slab

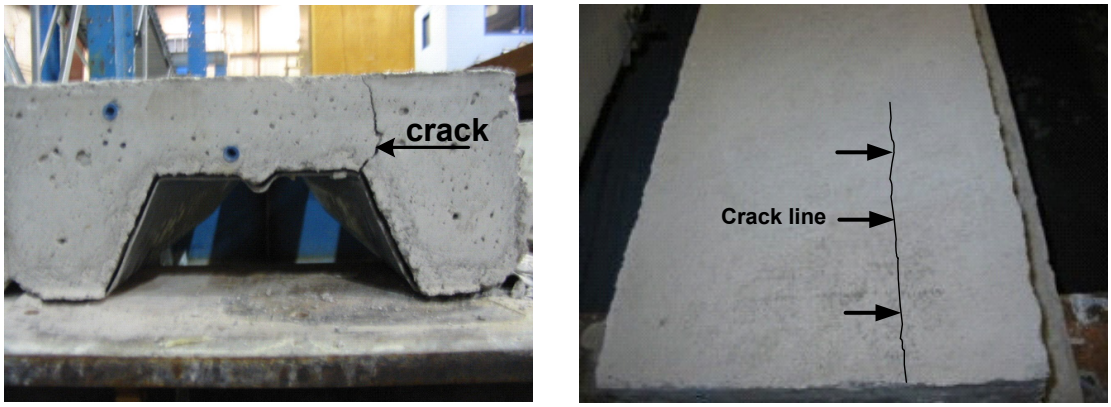

(a) (b)

Fig. 3.6 Longitudinal cracking of concrete along shear span for test A of specimen #20: 3VL16-8-5s-A
(a) End of slab, (b) Top view

3.4.2 Small scale series #2

The observed behavior suggested that most small scale slabs in series #2 failed earlier (or at lesser deflection) and were more brittle than the full scale specimens (refer graphs in Appendix C.2). However the amount of end slips for small scale specimens were compatible with the full scale specimens (refer graphs in Appendix C.3). The maximum loads of the small scale specimens were comparatively similar to the maximum loads of the full scale specimens. The magnitude of vertical separation along the sides of small scale specimens in series #2 was generally less than that in series #1. It was also observed that the pour stop welding in the compact specimens of series #2 failed in a sudden manner. After this failure, which also accompanied by loud sound especially in the specimens with 2VL decks, the slabs lost their strengths also in a sudden manner. This can be seen by steep descending lines of load-deflection graphs after reaching peak loads (refer graphs in Appendix C.2). Compact specimens with 2VL decks lost their strengths in a more abrupt manner than the compact specimens with 3VL decks.

3.5 Result for small scale series #1 – Factors effecting slab strength

3.5.1 Maximum loads and deflections

Maximum loads and the corresponding mid-span deflections and end slips, and the load at first end slip of 0.02 in. for small scale series #1 are tabulated in Table 3.2. Load-deflection graphs are given in the following sections when the effects of particular parameters are discussed. The load-end slip relationships are compiled in Appendix C.1.

3.5.2 Effect of web curling

The effect of restraining the webs from curling using angle straps for small scale specimens in series #1, which were tested at different shear spans, are illustrated in the load-deflection graphs in Fig. 3.7, Fig. 3.8 and Fig. 3.9. The graphs show that the strengthening of webs using angle straps significantly increased the capacity of the slabs specimens. The average increment of the maximum loads ranged between 30% and 48%.

Table 3.2 Quantitative results of small scale series #1 tests

Test number	Specimen ID	Shear span	Test	Maximum Load (psf)	Mid-span deflection at max. load (in.)	End slip at max. load (in.)	Load at first slip (0.02 in.) (psf)
13	3VL16-8-7.5	22	A	1250	0.796	0.187	840
			B	1320	0.84	0.169	760
14	3VL16-8-7.5	22	A	1010	0.976	0.175	420
			B	840	0.474	0.170	480
15	3VL16-8-7.5	26	A	1220	0.602	0.122	980
			B	1210	0.770	0.216	560
16	3VL16-8-7.5	26	A	910	0.855	0.206	420
			B	1070	0.829	0.159	510
17	3VL16-8-7.5	30	A	1540	0.689	0.14	1080
			B	1490	0.713	0.175	870
18	3VL16-8-7.5	30	A	1000	0.922	0.193	440
			B	1070	0.974	0.207	550
19	3VL16-8-6.5	22	A	1180	0.972	0.184	670
			B	1160	0.804	0.178	680
20	3VL16-8-5	22	A	860	0.923	0.13	510
			B	850	0.946	0.162	460

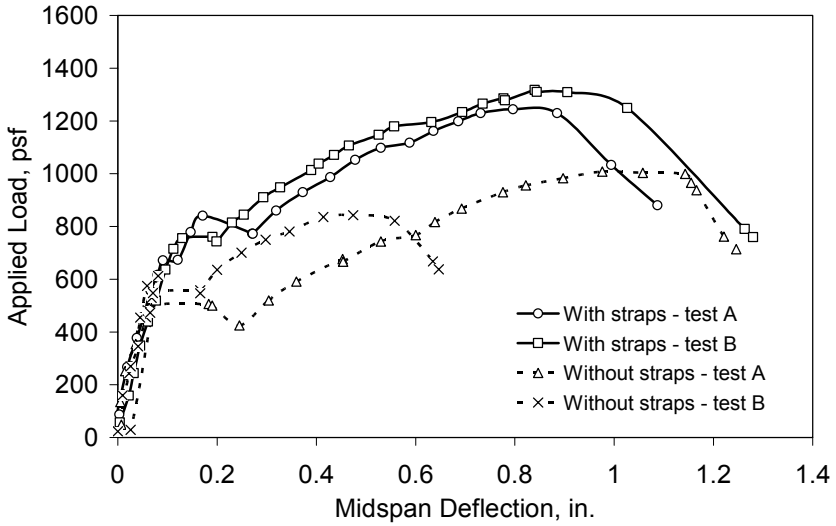

Fig. 3.7 Comparison of results for specimens with and without straps in series #1: 3VL16-8-7.5s – 22 in. shear span

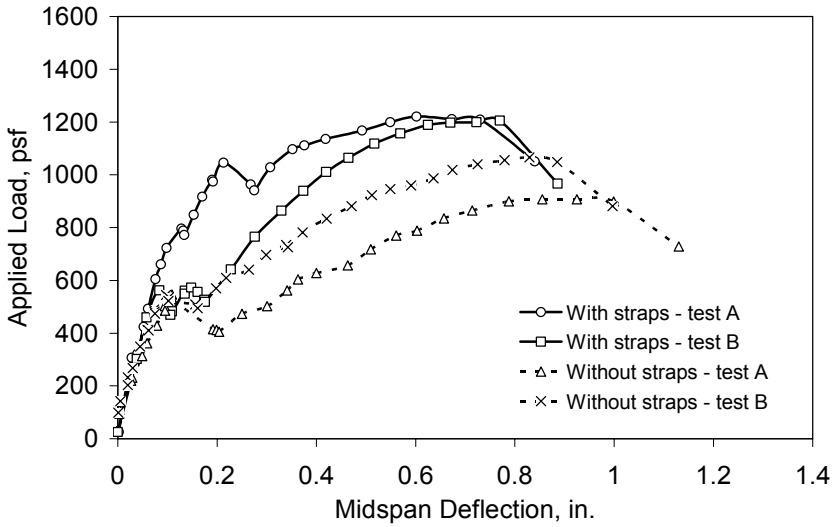

Fig. 3.8 Comparison of results for specimens with and without straps in series #1: 3VL16-8-7.5s – 26 in. shear span

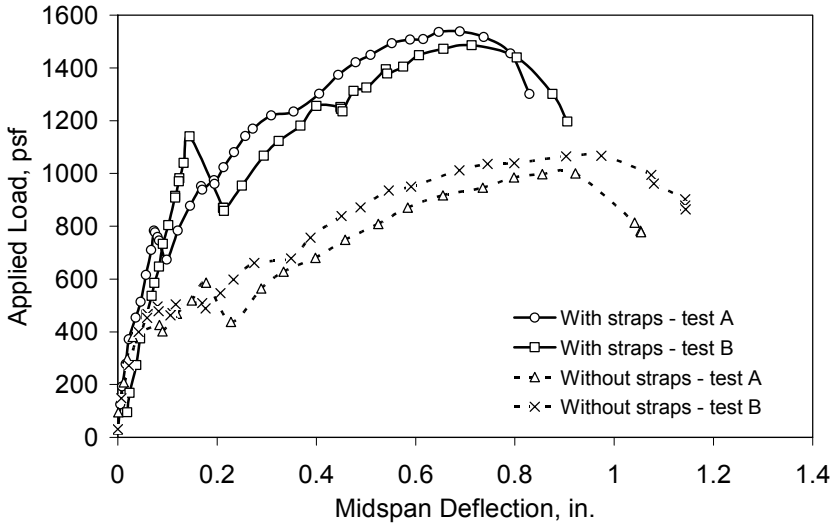

Fig. 3.9 Comparison of results for specimens with and without straps in series #1: 3VL16-8-7.5s – 30 in. shear span.

3.5.3 Effect of shear span length

The location of load position, which determines the length of shear span, can also influence the tests results. This is shown by the plot of maximum load versus shear span in Fig. 3.10. The specimens with straps were #13, #15 and #17 while for the ones with no straps were #14, #16 and #18 (refer Table 2.3). The plot indicates that the maximum load for slabs of similar configurations increased with increased shear span. This was true for specimens with and without straps. The actual variation (e.g. linear, parabolic, etc.) however was inconclusive because of insufficient data to develop any kind of a trend.

The maximum load of strapped specimens #15, which were tested at 26 in. shear spans, were relatively lower in relation to other compatible specimens tested at 22 in. and 30 in. shear spans. This load reduction can be attributed to the decks used in specimen #15, where the embossments on both webs were skewed toward the same direction, as already

noted in Sec. 2.7.2. These specimens suffered from a weaker shear resistance at the side where the embossments were skewed toward the slab end (refer Fig. 3.11). Obviously, the slip occurred at this section.

3.5.4 Effect of slab thickness

The capacities of slabs with different thicknesses are illustrated in Fig. 3.12. The plots depict the results of specimens #13, #19 and #20 where the thicknesses were 7.5 in., 6.5 in. and 5 in. respectively. These slabs were tested at 22 in. shear spans. As expected, the slab capacity increased with the thickness.

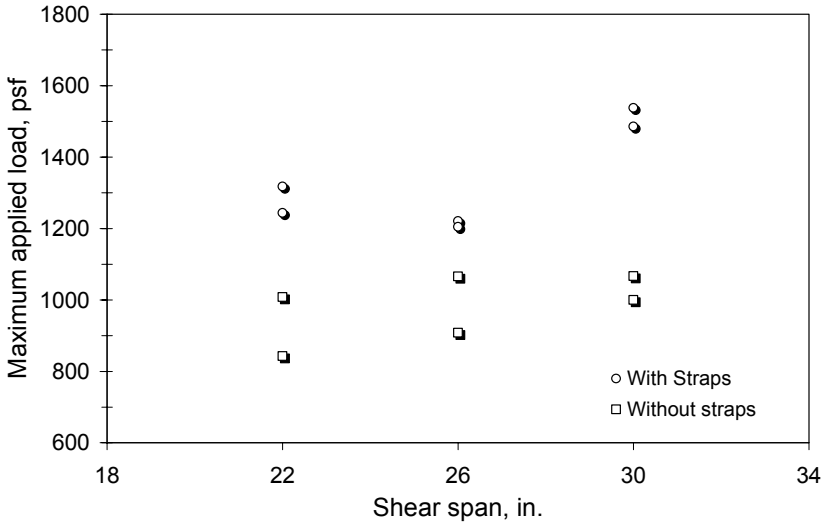

Fig. 3.10 Maximum applied load for 3VL16-8-7.5s series #1 tested at different shear spans.

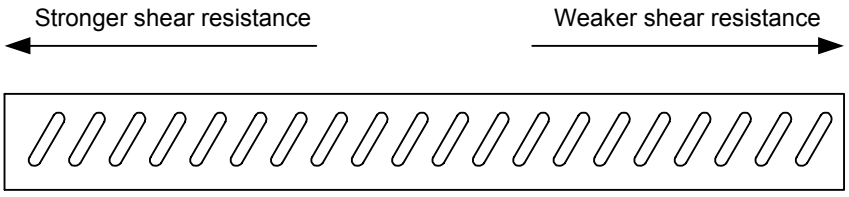

Fig. 3.11 Direction of embossments on both webs for specimen #15, small scale series #1

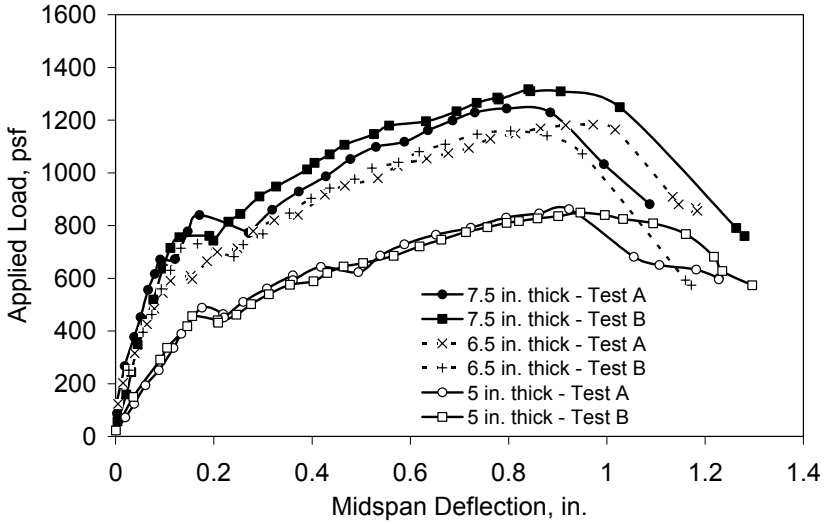

Fig. 3.12 3VL16-8 slabs with variable concrete thickness

3.5.5 Effect of end constraint

End anchorage details can affect the response of composite slab tests (Easterling and Young, 1992; Terry and Easterling, 1994). Three identical specimens from small scale test series #2 and one full scale test configuration, namely 3VL16-8-7.5, were compared to illustrate the effect of end anchorage. The first was specimen #17 from small scale series #1, which was supported by roller and pin details at the ends and without pour stop (see Sec. 2.7.2). The second specimen was #26 from small scale series #2 (see Table 2.4) where pour stops at both ends were welded to ½ in. thick and 4 in. wide steel plates, which were then supported on pin and roller supports. The third specimen was #27 from series #2 (see Table 2.4) where pour stops at both ends were welded to the support beams. The last was the compatible specimens from full scale test (specimen #5 Table 2.2) where the end detail was similar to specimen #27 series #2.

Load-deflection graphs for these specimens are shown in Fig. 3.13. The results show that the average maximum loads, as a ratio of the full scale slab maximum load, for

the first, second and third specimens are 0.69, 0.81 and 0.97 respectively. This indicated clearly that the end details could exert a significant effect on the performance of the slab. Furthermore, both small and full scale specimens whose end details were identical exhibited almost equal strength even though the small scale specimens were slightly stiffer in the beginning and failed faster than the full scale specimens.

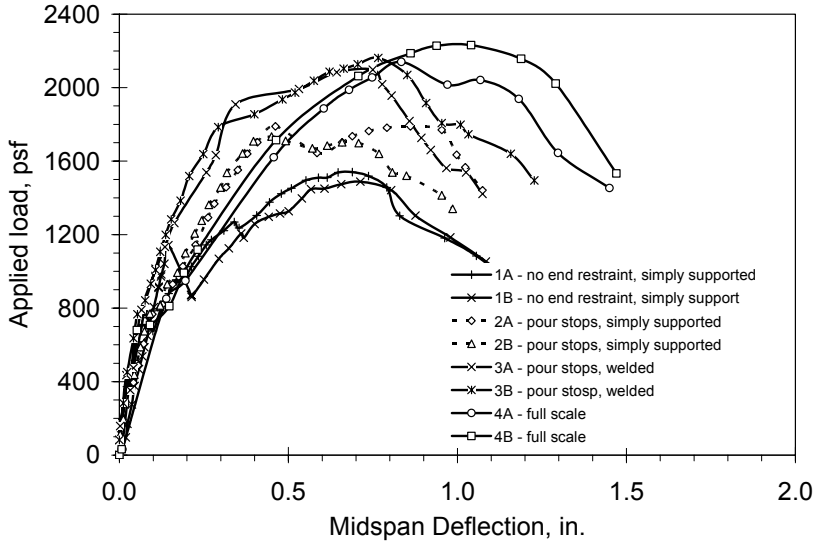

Fig. 3.13 3VL16-8-7.5 specimens with different end constraint

3.5.6 Effect of slab slenderness, L_s / d

Load-deflection results of specimen 3VL16-4-7.5, 3VL16-4-7.5, 3VL16-10-7.5, 3VL16-12-5 and 3VL16-14-5 from small scale series #2 are shown in Fig. 3.14 to illustrate the pattern of slab response due to variable slenderness. The maximum loads were plotted against slab slenderness, as shown in Fig. 3.15. The pattern of the maximum load was best fitted with a power function as shown in the figure. The slab capacity increased exponentially as the slenderness decreased.

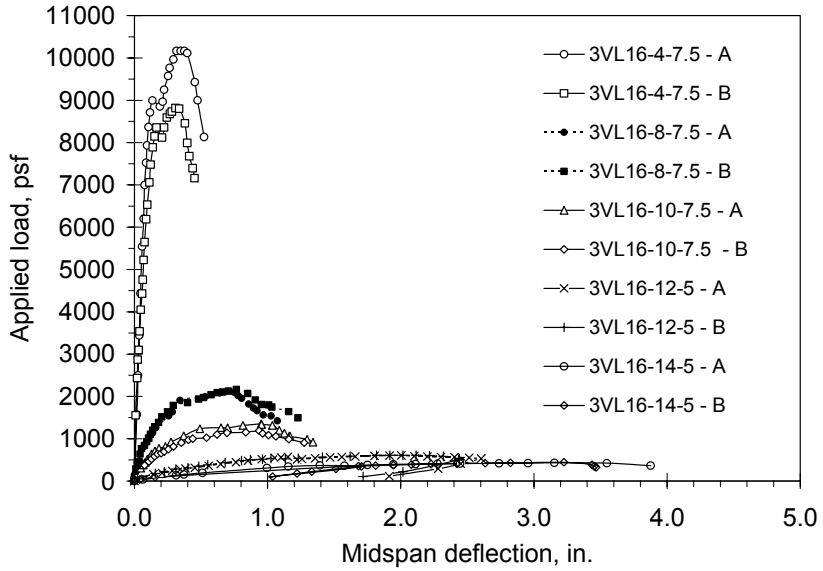

Fig. 3.14 Load-deflection for specimen 3VL16 with variable slenderness

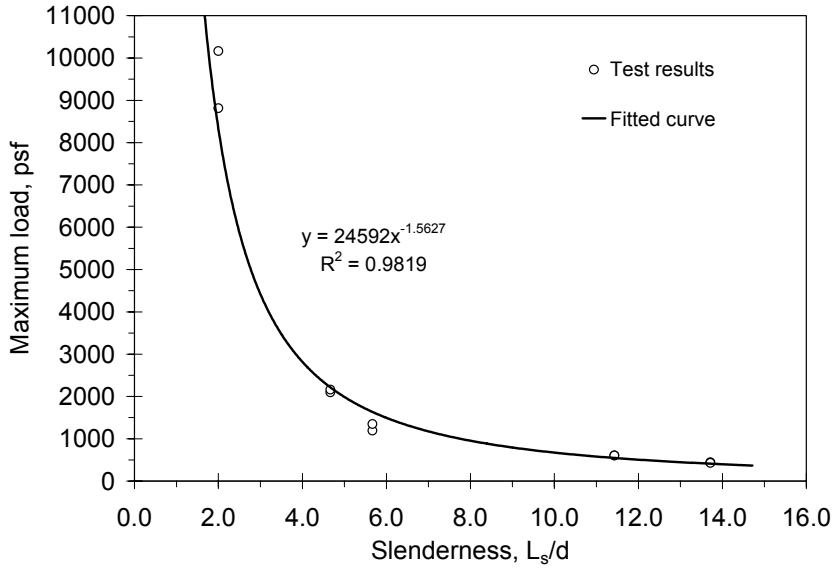

Fig. 3.15 Maximum load versus slenderness for 3VL16 specimens

3.6 Results of small scale tests series #2 and comparison with full scale tests

A summary of results in the form of maximum loads for series #2 and full scale tests are given in Table 3.3. The average maximum loads were compared and the values indicate that the performance of small scale tests is comparable with the full scale tests where the standard deviation of the ratio of average maximum small scale-to-full scale load

Table 3.3 Maximum load for small and full scale specimens

Specimen ID	Test	Full scale tests		Small scale tests		W_{us} / W_{uf}
		Max. load (psf)	Average max. load, W_{uf} (psf)	Max. load (psf)	Average max. load, W_{us} (psf)	
3VL20-8-7.5	A	1670	1660	1390	1380	0.83
	B	1650		1370		
3VL20-11-5	A	420	435	510	460	1.06
	B	450		410		
3VL18-8-7.5	A	1790	1815	1490	1530	0.84
	B	1840		1570		
3VL18-13-5	A	390	390	410	415	1.06
	B	390		420		
3VL16-4-7.5	A	-	-	10170	9495	-
	B	-		8820		
3VL16-8-7.5	A	2140	2185	2100	2130	0.97
	B	2230		2160		
3VL16-10-7.5	A	-	-	1350	1270	-
	B	-		1190		
3VL16-12-5	A	-	-	610	610	-
	B	-		610		
3VL16-14-5	A	380	395	430	435	1.10
	B	410		440		
2VL20-7-6.5	A	1540	1500	1600	1540	1.03
	B	1460		1480		
2VL20-9-4	A	460	470	480	470	1.00
	B	480		460		
2VL18-7-6.5	A	1940	1865	1830	1890	1.01
	B	1790		1950		
2VL18-11-4	A	430	450	450	450	1.00
	B	470		450		
2VL16-7-6.5	A	1860	2120	2620	2505	1.18
	B	2380		2390		
2VL16-12-4	A	480	475	470	485	1.02
	B	470		500		
					Mean	1.01
					Standard deviation	0.10

is 0.1 with the mean value of 1.01. Most results were within 10% difference, except for specimen 3VL20-8-7.5s and 3VL18-8-7.5s, which were weaker than the full scale specimens by 17%. This difference can be attributed to the full scale specimens being tested using the airbag as already explained in Sec. 2.6.6. The uniform pressure exerted by the airbag exerted extra clamping along the length of the slabs. The clamping restricted the movement of the concrete during slipping which eventually resulted in stiffness behavior. Full scale specimen 2VL16-7-6.5s was 18% stronger than full scale specimen. The difference was particularly due to outlying results of test A of the full scale specimen which was unexplainably weak compared to test B.

Graphs comparing the applied load versus mid-span deflection for full and small scale series #2 specimens are presented in Appendix C.2. There was an anomalous behavior of compact small scale specimens that deserves discussion. The graphs depict that all compact small scale specimens were stiffer than their corresponding full scale tests in load region below the maximum values. This behavior could be attributed to the welding of pour stops and steel decks at both ends of the small scale specimens, which might have provided additional resistance against rotation during the early stage of loading. In the full scale specimens, the amount of similar resistance existed only at the exterior supports, while at the interior supports, the continuity of the concrete was unable to provide the same resistance against rotation. This is because at the interior support, the concrete cracked at a very low load and the slabs were more flexible to move or rotate (refer also to discussion in Sec. 3.3). In addition to this, the amount of welding in the small scale specimens was larger than that in full scale specimens. In small scale specimens, two welding points per one ft wide specimen were provided compare to seven welding points per six ft wide in full scale

specimens. For slender specimens, the difference of stiffness between full and small scale specimens was insignificant because the behavior was mainly dominated by the slenderness and deflection of the specimens rather than the end conditions.

3.7 Load-end slip results

Fig. 3.16 shows typical graphs of the load versus end slip relationship obtained from small scale tests. The slip measured at the slab ends (location 1 as labeled in Fig. 2.19a) was of the same magnitude as the slip measured near point loads (location 2). As such, average values were considered and plotted as representative slip along the shear span. Load-end slip graphs for all small scale series #2 and full scale specimens are presented in Appendix C.3. Only slips at the failure sides of the specimens are presented. It should be noted also that for most results, slips were also recorded at the non failure ends of the specimens but for clarity, they are not presented in these graphs.

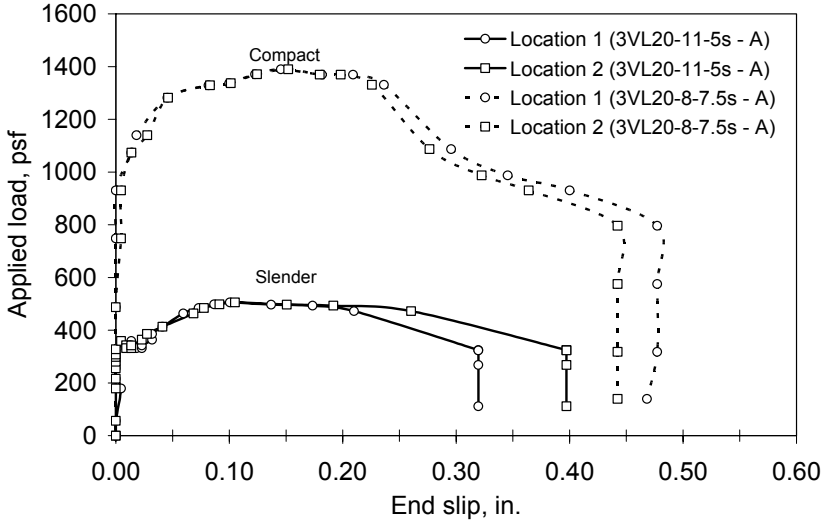

Fig. 3.16 Typical end slip measured at location 1 (end of slab) and location 2 (near applied load) for slender and compact slabs

3.8 Load at deflection limit

Deflection is the main criteria for the serviceability limit state. The applied loads from the tests at a deflection equal to the *span*/360 are presented in Table 3.4. A comparison with a 50 psf minimum design load is also given in Table 3.4. The applied loads for compact slabs excluding 3VL16-4-7.5s were between 14 to 30 and 24 to 38 times greater than the design load for full and small scale respectively, while for slender slabs the ranges were between 3 to 7 and 3 to 6 times for full and small scale respectively. The ranges suggested that the small scale specimens were stiffer than the full scale specimens for the *span*/360 deflection limit. This result further confirmed the discussion in Sec. 3.6. It is also obvious that slabs with thicker gage decks could take more loads than those with thinner decks at the specified deflection limits.

3.9 Failure mode

Eurocode 4 (1994) defines a ductile failure to have occurred when the failure load exceeds the load causing the first recorded end slip by 10%. As mentioned by Veljkovic (1998), the value of the first end slip considered in Eurocode 4 is 0.02 in. (0.5 mm). If the maximum load is reached at a mid-span deflection exceeding *span*/50, then the failure load shall be taken as the load at a mid-span deflection of *span*/50.

Based on the first recorded end slip of 0.02 in., the failure modes for full and small scale tests were determined and are listed in Table 3.5. From the results, two of the full scale specimens namely 3VL18-13-5f and 3VL16-14-5f had maximum loads exceeding the *span*/50 deflection limit. For specimen 2VL18-11-4f-A and B and 3VL20-11-5f-B, the first initiation of end slip and its subsequent growth occurred after the applied loads had reached the maximum values and significant deflection and rotation had taken place. It was

concluded that the failure for these specimens was a combination of slip and flexure and occurred in a ductile manner.

Table 3.4 Load at *span*/360 deflection limit and comparison with design load

Specimens	Tests	Load at *span*/360 limit, W_s (psf)		W_s/50 full scale	W_s/50 small scale
		Full scale tests	Small scale tests		
3VL20-8-7.5	A	850	1200	17.0	24.0
	B	730	1220	14.6	24.4
3VL20-11-5	A	250	220	5.0	4.4
	B	230	300	4.6	6.0
3VL18-8-7.5	A	1150	1250	23.0	25.0
	B	1100	1210	22.0	24.2
3VL18-13-5	A	210	190	4.2	3.8
	B	230	150	4.6	3.0
3VL16-4-7.5	A	-	7800	-	156.0
	B	-	9000	-	180.0
3VL16-8-7.5	A	1080	1550	21.6	31.0
	B	1160	1700	23.2	34.0
3VL16-10-7.5	A	-	870	-	17.4
	B	-	1010	-	20.2
3VL16-12-5	A	-	310	-	6.2
	B	-	300	-	6.0
3VL16-14-5	A	170	180	3.4	3.6
	B	160	150	3.2	3.0
2VL20-7-6.5	A	1000	1380	20.0	27.6
	B	900	1430	18.0	28.6
2VL20-9-4	A	370	210	7.4	4.2
	B	310	230	6.2	4.6
2VL18-7-6.5	A	1200	1650	24.0	33.0
	B	1150	1700	23.0	34.0
2VL18-11-4	A	260	230	5.2	4.6
	B	240	260	4.8	5.2
2VL16-7-6.5	A	1490	1900	29.8	38.0
	B	1500	1900	30.0	38.0
2VL16-12-4	A	240	180	4.8	3.6
	B	220	170	4.4	3.4

Table 3.5 Failure mode of the specimens

Specimens	Span	Full scale tests				Small scale tests			
		Failure load, W_{uf} (psf)	Load at 1st slip, W_s (psf)	W_{uf}/W_s	Failure mode	Failure load, W_{us} (psf)	Load at 1st slip, W_s (psf)	W_{us}/W_s	Failure mode
3VL20-8-7.5	A	1670	1400	1.19	Ductile	1390	1150	1.21	Ductile
	B	1650	1300	1.27	Ductile	1370	1100	1.25	Ductile
3VL20-11-5	A	420	310	1.35	Ductile	510	350	1.46	Ductile
	B	450	-	-	Ductile	410	320	1.28	Ductile
3VL18-8-7.5	A	1790	1200	1.49	Ductile	1490	1170	1.27	Ductile
	B	1840	1060	1.74	Ductile	1570	1220	1.29	Ductile
3VL18-13-5	A	390	290	1.34	Ductile	410	350	1.17	Ductile
	B	390	290	1.34	Ductile	420	270	1.56	Ductile
3VL16-4-7.5	A	-	-	-	-	10170	8900	1.14	Ductile
	B	-	-	-	-	8820	7000	1.26	Ductile
3VL16-8-7.5	A	2140	1450	1.48	Ductile	2100	1590	1.32	Ductile
	B	2230	1350	1.65	Ductile	2160	1520	1.42	Ductile
3VL16-10-7.5	A	-	-	-	-	1350	1030	1.31	Ductile
	B	-	-	-	-	1190	830	1.43	Ductile
3VL16-12-5	A	-	-	-	-	610	500	1.22	Ductile
	B	-	-	-	-	610	510	1.20	Ductile
3VL16-14-5	A	380	280	1.36	Ductile	430	370	1.16	Ductile
	B	410	330	1.24	Ductile	440	160	2.75	Ductile
2VL20-7-6.5	A	1540	1200	1.28	Ductile	1600	1400	1.14	Ductile
	B	1460	1100	1.33	Ductile	1480	1220	1.21	Ductile
2VL20-9-4	A	460	350	1.31	Ductile	480	330	1.45	Ductile
	B	480	380	1.26	Ductile	460	420	1.10	Ductile
2VL18-7-6.5	A	1940	1200	1.62	Ductile	1830	1420	1.29	Ductile
	B	1790	1200	1.49	Ductile	1950	1730	1.13	Ductile
2VL18-11-4	A	430	-	-	Ductile	450	280	1.61	Ductile
	B	470	-	-	Ductile	450	360	1.25	Ductile
2VL16-7-6.5	A	1860	1800	1.03	Brittle	2620	2500	1.05	Brittle
	B	2380	1900	1.25	Ductile	2390	1900	1.26	Ductile
2VL16-12-4	A	480	420	1.14	Ductile	470	350	1.34	Ductile
	B	470	350	1.34	Ductile	500	280	1.79	Ductile

Other specimens including all small scale tests failed by shear bond but also exhibited ductile behavior, except for 2VL16-7-6.5f-A and 2VL16-7-6.5s-A which, according to the definition, failed in the brittle manner. It is suspected that these particular specimens had undetected imperfections because their results differed too greatly, and unexplainably, from the compatible specimens.

3.10 Strain gage results for full scale specimens

It was not possible to observe yielding during the tests. For yielding measurement it was assumed here that the deck began to yield at the strain, $\varepsilon_y = F_y / E_s$ where F_y is the deck yield stresses obtained from coupon tests and E_s is the modulus of elasticity taken as 29500 ksi. At this strain value, the corresponding yield loads were read from the load-strain plots at mid-span and the values are presented in Table 3.6. For all full scale specimens, yielding of steel decks was observed at the bottom flanges. The top flange strains did not undergo tension yielding because the strains reduced after slip occurred. This slip resulted in the formation of double neutral axes, one for the partially composite action and the other was for the remaining strength of the deck.

Table 3.6 Loads measured at yielding of steel decks for full scale tests

Specimens	Span	Yield strain, ε_y	Load at yield strain, W_{et} (psf)	Failure load, W_{uf} (psf)	W_{uf} / W_{et}
3VL20-8-7.5	A	0.00183	1120	1670	1.49
	B		1050	1650	1.57
3VL20-11-5	A	0.00183	370	420	1.14
	B		380	450	1.18
3VL18-8-7.5	A	0.00163	1430	1790	1.25
	B		1370	1840	1.34
3VL18-13-5	A	0.00163	310	390	1.26
	B		290	390	1.34
3VL16-8-7.5	A	0.00173	1700	2140	1.26
	B		1780	2230	1.25
3VL16-14-5	A	0.00173	330	380	1.15
	B		310	410	1.32
2VL20-7-6.5	A	0.00176	1450	1540	1.06
	B		1420	1460	1.03
2VL20-9-4	A	0.00176	440	460	1.05
	B		430	480	1.12
2VL18-7-6.5	A	0.00166	1800	1940	1.08
	B		1700	1790	1.05
2VL18-11-4	A	0.00166	410	430	1.05
	B		400	470	1.18
2VL16-7-6.5	A	0.00159	1780	1860	1.04
	B		2180	2380	1.09
2VL16-12-4	A	0.00159	430	480	1.12
	B		380	470	1.24

3.11 Concluding remarks

From the observation and test data as presented above, the following conclusions can be made;

1) The continuity of the slab without negative reinforcement did not provide restraint against rotation. However the end slip could be delayed from occurring.

2) The ductility of the steel deck prevented the slab from collapsing after ultimate load was achieved.

3) When the slab failed by shear bond, the concrete slipped along the shear span causing cracking at the critical section. The crack grew until top fiber. The concrete did not fail by crushing.

4) Relative slip can be assumed uniform along the shear span.

5) Slabs with relatively shallow deck failed more abruptly in a more brittle fashion than with deeper decks.

6) Edge curling had a significant influence on the slab strength and behavior. Angle straps can provide sufficient restraint to the edge web, thus enabling small scale specimens to behave in a manner similar to full scale specimens.

7) Concrete thickness, embossment orientation, end anchorage and support type affect the response and behavior of small scale specimens. Concrete cover that is too thin may result in longitudinal cracking along the shear span. Embossments on opposite webs that are oriented in the same direction can weaken the slab specimen. Specimens anchored with pour stops welded to fixed supports were stronger than those bearing on the simple supports.

8) Thickness and shear span influenced the slab capacity significantly.

9) Slender slabs sustained load at least three times larger than the load at a deflection equal to *span*/360. Compact slabs sustained load approximately 20 times the load reached at a deflection of *span*/360.

10) All specimens except one exhibited ductile failure.

11) Strain gage readings indicated that the steel deck bottom flange yielded at a load below the ultimate load.

12) With sufficient number of angle straps and with compatible end condition, the small scale specimen developed in this experimental study can be used as an alternative to the full scale specimen.

4 Analytical methods

4.1 Introduction

It has been recognized that the mechanism of horizontal shear resistance between the steel deck and the concrete in composite slabs is complex. Because of the complexity, it is not possible to develop an analytical method that is suitable for all slab conditions without using data from tests. Because of the need for test data, it is imperative to develop an efficient, simple and economical testing method such as the one developed in this research. In addition to being simple and cost effective, the test must more importantly produce data that is suitable for use with analytical methods in all conditions. Otherwise the testing method itself will have less practical value. This chapter deals with putting the small scale test data into practical use.

4.2 Objective

The main objective of this portion of the research was to verify that the small scale test procedure developed and presented in the previous chapters is an admissible tool for use in the design of composite slabs. The most established design methods to date, namely the *m-k* (ASCE, 1992; BS-5950, 1994; Eurocode 4, 1994) and the PSC (Eurocode 4 1994) methods, were chosen for this study. The second objective was to develop a procedure for calculating a shear bond stress versus slip relationship from the same test for use in modeling the slab using the FE method. In doing so, two calculation procedures were

proposed, namely the work method and the force equilibrium method. By introducing these procedures the practical use of the small scale test can be diversified.

In the following sections, methods of analysis available in the literature are briefly reviewed. Then the *m-k* and the PSC methods are discussed in detail. After that, the work method and force equilibrium method are presented. Small scale test data obtained in the previous chapter are then analyzed with these methods and the results are compared. The application of the shear bond stress-slip property in the FE analysis is studied in the next chapter.

4.3 Review of the analysis and design methods

4.3.1 The shear bond (*m-k*) method

The first standard method for composite slab design that is widely accepted and has been implemented in many specifications around the world is the shear bond method. The development of this method began from the work of Schuster (1970) and later was improved by Porter et al. (1976), Porter and Ekberg (1971, 1975a, 1975b). This method uses full scale test data where the slab shear strength is related linearly with the slab geometry. The linear equation uses *m* and *k* as variables for the slope and intercept, hence they became the name for the method. Because of its accuracy and simplicity the *m-k* method was chosen for analyzing the small scale test data developed in this research. The *m-k* method according to (ASCE, 1992) and (Eurocode 4, 1994) are presented in detail in the Sec. 4.4.

The major drawback of the *m-k* method is that it is semi-empirical, in that it does not provide a clear mechanical model that can separate factors that contribute to the performance of the composite slabs. These factors include shear bond strength, end

anchorage, frictional force at supports and additional reinforcements. The *m-k* method depends heavily on full scale test data in which different series of full-scale tests are needed for each new sheeting profile, sheeting thickness, embossment type, end anchorage, etc. This design process is costly, tedious and less than desirable to deck manufacturers because prototypes of all new products have to be built and tested at full-scale before the profile can be evaluated. Additional drawbacks associated with the lack of a mechanical model are discussed by Bode and Sauerborn (1992).

4.3.2 The Partial Shear Connection (PSC) method

To overcome the deficiencies of the *m-k* method, especially the lack of a mechanical model that reflects the influence of composite slab parameters, and to reduce dependency on full scale tests, researchers in Europe developed the partial shear connection (PSC) method. This method was first proposed by Stark (1978) and subsequently improved by Stark and Brekelmans (1990), Bode and Sauerborn (1992), Bode et al. (1996), and Bode and Dauwel (1999). The method was adopted in Annex E of Eurocode 4 (1994) as an alternative to the *m-k* method. It became part of the Eurocode 4 design specification in the newer edition (Eurocode 4, 2001). Because the PSC method uses a sound mechanical model and has potential for inclusion into the ASCE specification (ASCE, 1992), it was also chosen for analyzing the small scale test data developed in this research. Details of the PSC method are given in Sec. 4.5.

4.3.3 Other methods

Research at West Virginia University resulted in an empirical approach to calculate the bending strength for composite slabs (Luttrell and Davidson, 1973; Luttrell and Prasannan, 1984; Luttrell, 1986). It was implemented in Appendix D of the ASCE (1992)

standard as a complement to the *m-k* method discussed earlier. In this method, the theoretical bending moment capacity of the slab is calculated based on the assumption that the deck bottom flange yields. The first yield moment is modified by coefficients that are a function of the shear transfer anchorage forces that developed along the shear span. The modification factors were empirically based, hence the application is limited to certain types of deck profiles and embossments. Experimental work reported on trapezoidal profiles with embossment sizes and patterns outside the prescribed limits gave satisfactory results when calculated using this method (Shen, 2001). On the other hand, Wright and Evans (1990) reported that the method did not provide acceptable results for slabs constructed with deck profiles available in the United Kingdom. Despite producing less accurate results, this method is still useful especially for predicting the slab strength during product development and for predicting maximum load before the actual test is carried out.

Research done at the University of Waterloo resulted in another empirical equation for predicting the strength of composite slabs that fail by shear bond (Seleim, 1979; Seleim and Schuster, 1985). The equation, which requires multi linear regression analysis, is based on experimental evidence of composite slabs exhibiting early end slip prior to ultimate load and it contains steel deck thickness as a parameter. The authors indicate that the presence of the steel deck thickness parameter can result in a reduction of up to 75% of the required number of laboratory performance tests. The method is incorporated in the CSSBI (1996) design specification.

An alternative formulation to predict the strength of composite slabs for design purposes is reported by Heagler et al. (1991). The method uses a traditional reinforced concrete flexural model and also includes the influence of shear stud strength at the slab

ends. Linear interpolation can be made between the value for full nominal moment capacity (completely studded slab) and first yield moment capacity (non studded slab) for slabs having insufficient number of shear studs (Terry and Easterling, 1994). The method does not directly consider or account for the behavior of the interface between the steel deck and the concrete.

Patrick (1990) developed a method for design of composite slabs that does not require full-scale slab tests. The method uses the average mechanical interlocking (shear bond) and friction at the support and is applicable only to ductile behavior. The shear resistance parameters are obtained from slip block test as discussed in Sec. 2.3.6. By inclusion of the friction force at the support, the calculated slab strength is increased. The advantage of Patrick's approach is that the interface property was obtained through elemental tests instead of full-scale performance tests. This could significantly reduce the product development cost. However the method requires moment curvature analysis, which has to be performed at small discretized layers of the slab section under varying load levels and at small intervals along the length of the slab to generate a moment envelope for use in design. This requires a lot of computer programming effort, without which the method is rendered impractical for regular practice.

Another method of design was proposed by Veljkovic (1996b). The method uses three parameters, namely, the mechanical interlocking resistance, coefficient of friction, and a reduction function for mechanical interlocking due to high strain in the sheeting. These parameters are obtained from elemental tests (see Sec. 2.3.9) hence the method is called the Three Parameters Partial Connection Strength Method (3P PCSM). Using these parameters a FE analysis is performed on slabs with variable slenderness. Regression

analysis is then carried out on the FE results to obtain two correction functions. The first function accounts for the difference between the real distribution of stress in the concrete and the assumed rectangular stress block in the analysis (uncertainty in lever arm and tensile force). The second function accounts for the difference between the real (non-uniform) distribution of longitudinal shear stress at the sheeting and concrete interface and the assumed uniform distribution in the analysis. All parameters obtained from the elemental tests and the correction functions obtained from the FE analysis are then used in a design equation for calculating the slab strength, expressed in terms of reaction force. Compared to the Eurocode's PSC method, the results from this procedure showed a better agreement with the *m-k* method. The design equation was simple to use, however because the design parameters have to be derived from elemental tests and FE analysis, the method is cumbersome for use in design practice.

In a subsequent study, Veljkovic (1998, 2000) found that the longitudinal shear resistance of the slab increased as the loading became more uniform. The increment of the resistance with respect to 2-point loading was 20%, 30% and 40% for 4-point, 8-point and 16-point loading respectively. To account for the influence of the load arrangement and the distribution of horizontal shear when the connection becomes less ductile, he modified the 3P PCSM method. The modified method uses a new concept called transfer length, which is defined as the length between the section of maximum bending moment and the support. The transfer length needed to cause yielding of the sheeting together with the resistance produced by the friction force at the support are used to construct the moment resistance envelope, from which the slab design can be done. Veljkovic indicated that this method is suitable for both ductile and brittle shear connection.

Other methods for calculating the strength of composite slabs can be found in the literature (Plooksawasdi, 1977; Wright and Evans, 1990; Widjaja and Easterling, 1996; Widjaja, 1997; Schumacher et al., 2000; Crisinel and Marimon, 2003). None of these methods are developed further in this research.

4.4 Details of the *m-k* method

In the *m-k* method, the strength of a composite slab, which is measured by an applied shear force, is related to the geometry of the slab by Eq. 4.1 (ASCE, 1992);

$$\frac{V_e}{bd\sqrt{f'_{ct}}} = \frac{m\rho d}{l'_i\sqrt{f'_{ct}}} + k \tag{4.1}$$

where

V_e = maximum experimental shear at failure obtained from full scale slab tests (not including weight of slab)

b = unit width of slab

d = effective slab depth measured from extreme concrete compression fiber to the centroidal axis of full cross section of steel deck

m = slope of reduced experimental shear-bond line

ρ = ratio of steel deck area to effective concrete area, $\frac{A_s}{bd}$

k = ordinate intercept of reduced experimental shear-bond line

l'_i = length of shear span in inches;

f'_{ct} = compressive test cylinder strength of concrete at time of slab testing.

The values of *m* and *k*, which represent the shear bond characteristics of a particular deck profile, are determined from a series of full-scale tests, where the test results are plotted with $\frac{V_e}{bd\sqrt{f'_{ct}}}$ on the y-axis and $\frac{\rho d}{l'_i\sqrt{f'_{ct}}}$ on the x-axis as shown in Fig. 4.1.

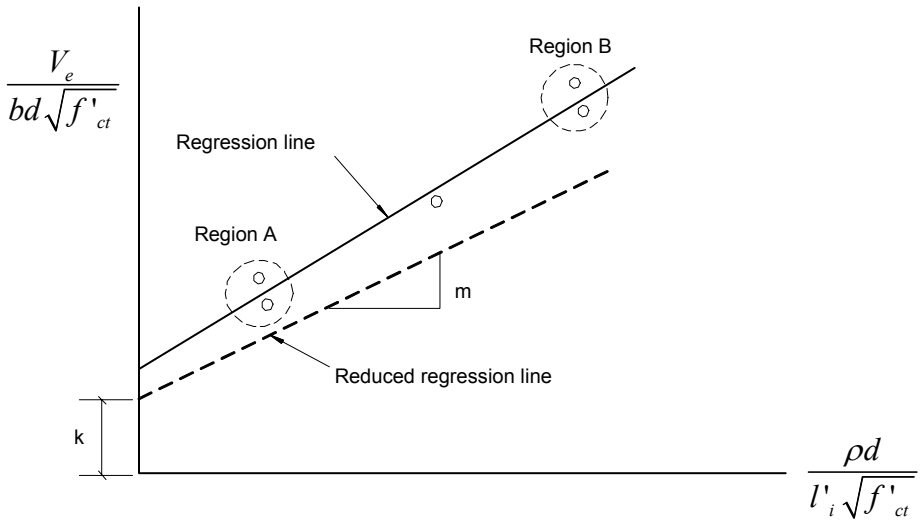

Fig. 4.1 Typical shear bond plot showing the regression line for *m* and *k*

Once the test results for Region A (slender specimens) and Region B (compact specimens) are obtained, a linear regression is performed on the data and the *m* and *k* values are obtained. For design purpose the slope and intercept are reduced as shown. The ASCE (1992) specifies the reduction of 10% or 15% depending on the number of tests. The reduction is to account for test variations and also to assure that the line approaches a lower bound for experimental values and is therefore somewhat conservative. To obtain reliable data, a minimum of two specimens each for Region A and B are suggested by the ASCE (1992) but three each are more recommended. Porter and Ekberg (1976) suggested using

data points from at least eight tests of each deck thickness and product type while the BS 5950 (1994) and Eurocode 4 (1994) suggest six tests.

To design other slabs whose length and thickness fall between the two test regions the *m* and *k* values are applied into Eq. 4.2;

$$\Phi V_n = \Phi\left[bd\left(\frac{m\rho d}{l'_i} + k\sqrt{f'_c} \right) + \frac{\gamma W_s l_f}{2} \right] \tag{4.2}$$

where,

Φ = strength reduction factor

V_n = nominal shear bond strength, lbs per ft of width

f'_c = specified compressive strength of concrete, psi

γ = coefficient for proportion of dead load added upon removal of shore

W_s = weight of slab

l_f = length of span or shored span, ft. The last term in the equation is to account for the shoring load if applicable.

Eurocode 4 omits the concrete strength from the equations because it may give unsatisfactory values for *m* and *k* if the concrete strength varies widely within a series of tests (Johnson, 1994). Many researchers have reported that the concrete strength does not have a significant effect on the slab capacity (Seleim and Schuster, 1985; Luttrell, 1987; Daniels, 1988; Bode and Sauerborn, 1992; Veljkovic, 1994). Eurocode 4 does not include the shoring removal term as in Eq. (4.2) but specifies that the slab shall be cast on "full prop." The *m*-*k* equation according to Eurocode 4 (2001) is;

$$\frac{V}{bd} = m\left(\frac{A_s}{bL_s}\right) + k \tag{4.3}$$

where,

L_s = shear span length, and other variables are similar to Eq. 4.1.

4.5 Details of the PSC method

In the PSC method the slab is assumed to fail in horizontal shear where the concrete can slip relative to the steel deck considerably without losing the load carrying capacity. In other word, the horizontal shear stress at the slip surface remains constant. This assumption requires a ductile shear failure.

The procedure for the PSC method begins with generating a theoretical partial interaction curve of $\frac{M}{M_{p.Rm}}$ versus η as typically shown in Fig. 4.2(a). The calculations for the curve are made using measured dimensions and strength of concrete and steel components. The x-axis of the partial interaction curve, η, is the degree of interaction, for which the values are chosen at fixed intervals from 0 to 1. The moment resistance of composite slabs under partial interaction is denoted by M, while $M_{p.Rm}$ is the moment resistance of composite slabs under full interaction.

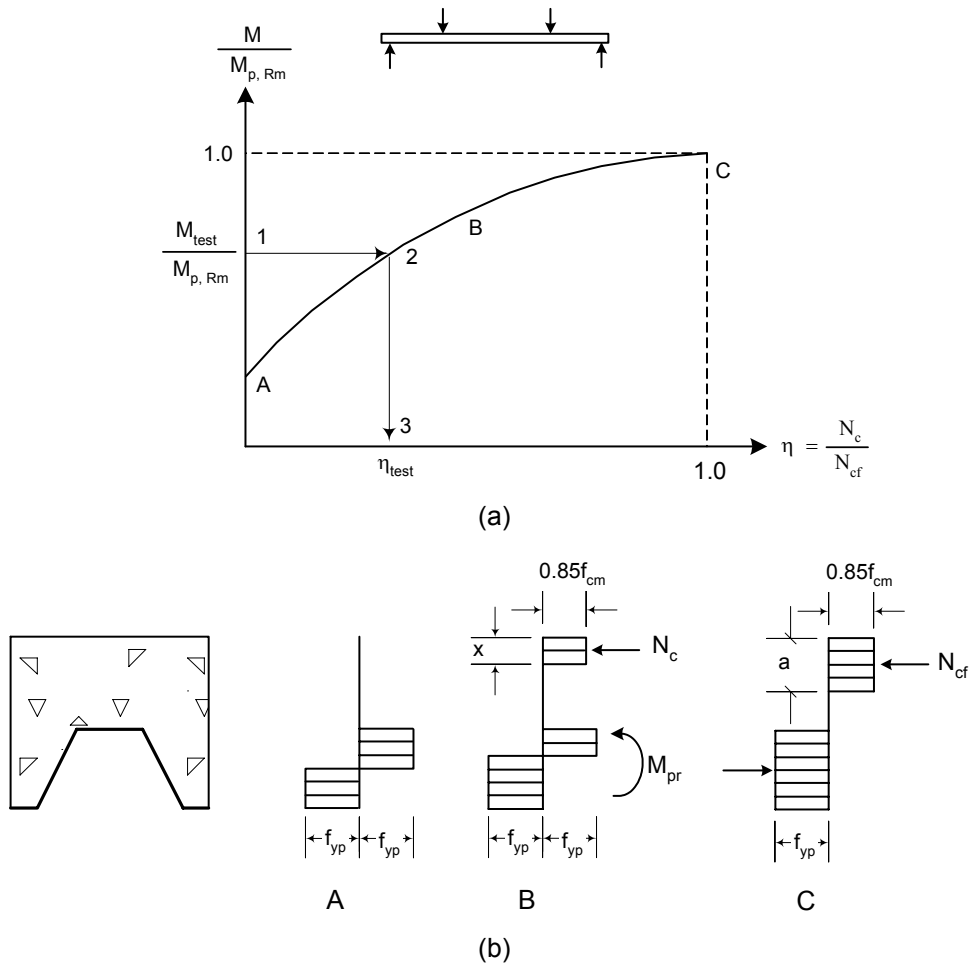

Fig. 4.2 Partial shear connection method
(a) Partial interaction curve, (b) Stress distributions at points A, B and C (Eurocode, 1994)

Points A and C in the curve of Fig. 4.2(a) are two extreme cases corresponding to no interaction and full interaction where $M = 0$ and $M = M_{p.Rm}$ respectively and the corresponding stress blocks are depicted in Fig. 4.2(a) and (c). The partial interaction state lies in between these two points, such as at point B where M is calculated following the stress block of Fig. 4.2(b);

$$M = N_c z + M_{pr} \tag{4.4}$$

where,

N_c = concrete compressive force under partial interaction

z = moment arm whose value depends on the degree of shear connection

M_{pr} = reduced moment capacity of the steel deck

The concrete compressive force under partial interaction is a fraction of the concrete compressive force under full interaction, N_{cf} and the amount depends on the degree of interaction;

$$N_c = \eta N_{cf} \tag{4.5}$$

The moment arm of Eq. 4.4 is;

$$z = h_t - 0.5x - e_p + (e_p - e)\eta \tag{4.6}$$

where

h_t = total slab thickness.

x = depth of concrete compressive zone.

e_p = distance from the plastic neutral axis of the steel deck to its extreme bottom fiber.

e = distance from the centroid of the effective area of the sheeting to its extreme bottom fiber.

The steel deck assumes dual functions under partial composite interaction. First, it serves as tension reinforcement in composite action, which is already considered in the first term of Eq. 4.4. Second it serves as an independent bending element where the deck bends about its own axis. The bending capacity however is reduced from the full capacity depending on the amount of composite action. The reduced moment, M_{pr}, is calculated by;

$$M_{pr} = 1.25 M_{pa}\left[1-\eta\right] \le M_{pa} \tag{4.7}$$

where,

M_{pa} = plastic moment of the effective cross section of the steel deck.

The depth of concrete compressive zone, x in Eq. 4.6 is given by;

$$x = \frac{N_c}{b(0.85 f_{cm})} \le h_c \tag{4.8}$$

where,

b = width of slab

f_{cm} = concrete compressive strength

h_c = thickness of concrete cover above the steel deck.

$M_{p.Rm}$ in the y-axis of partial interaction curve is the moment resistance of composite slabs under full interaction. It is given by;

$$M_{pRm} = N_{cf}(d_p - 0.5a) \tag{4.9}$$

where,

d_p = effective depth of the slab

a = depth of concrete compressive zone at full interaction, $a = \dfrac{A_p f_{yp}}{0.85 f_{cm} b}$

N_{cf} in Eq. 4.5 and 4.9 is the concrete compressive force for full interaction;

$$N_{cf} = A_p f_{yp} \tag{4.10}$$

where,

A_p = effective area of the steel deck

f_{yp} = yield strength of the steel sheeting.

Equation 4.4 to 4.10 are applicable to under reinforced sections where the neutral axis lies in the concrete, which is the case for shallow depth profiles.

The next step is obtaining the degree of interaction from the partial interaction curve just plotted. In this step, full scale tests are required from which the maximum bending moment, M_{test} is obtained. Using M_{test}, the degree of interaction η_{test} is read from the curve as shown by path 1-2-3 in Fig. 4.2(a). Knowing the degree of interaction the ultimate shear stress, τ_u can now be calculated;

$$\tau_u = \frac{\eta_{test} N_{cf}}{b(L_s + L_0)} \tag{4.11}$$

where,

L_s = shear span length

L_o = overhanging length beyond support

To satisfy the required level of confidence, Eurocode 4 suggests at least six full scale tests be performed to obtain the characteristic value of shear strength, $\tau_{u.Rk}$. Eurocode 4 allows for taking the minimum value of all tests, reduced by 10%. The design strength of the shear connection, $\tau_{u.Rd}$ is then obtained by dividing the characteristic strength with the partial safety factor, γ_v;

$$\tau_{u.Rd} = \frac{\tau_{u.Rk}}{\gamma_v} \tag{4.12}$$

Once the design shear strength is known, the design partial interaction curve or more exactly the design moment envelope for the particular deck profile can be drawn using Eq. 4.13 through 4.18 given below. The plot is illustrated in Fig. 4.3.

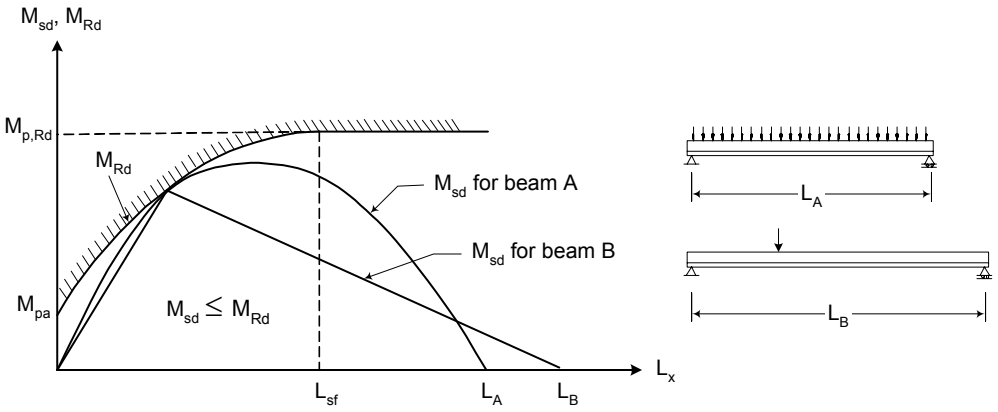

Fig. 4.3 Partial interaction diagram

$$M_{Rd} = N_c z + M_{pr} \tag{4.13}$$

$$N_c = bL_x\tau_{u.Rd}; \qquad L_x \le L_{sf} \tag{4.14}$$

$$L_{sf} = \frac{N_{cf}}{b\tau_{u.Rd}} \tag{4.15}$$

$$N_{cf} = A_p \frac{f_{yp}}{\gamma_{ap}} \tag{4.16}$$

$$z = h_t - 0.5x - e_p + (e_p - e)\frac{N_c}{N_{cf}}; \qquad N_c \le N_{cf} \tag{4.17}$$

$$x = \frac{N_c}{b(0.85\frac{f_{ck}}{\gamma_c})} \le h_c \tag{4.18}$$

where,

M_{Rd} = design value of resisting bending moment in partial interaction mode (ie. moment envelope)

$M_{p,Rd}$ = maximum resisting moment for the particular profile at full interaction

L_x = distance from the support representing beam length

L_{sf} = shear span length required for full shear connection

γ_v = partial safety factor for full shear resistance

γ_{ap} = partial safety factor for profile steel sheeting

γ_c = partial safety factor for concrete

f_{ck} = characteristic compressive strength of concrete, and other variables are as defined before.

The design partial interaction curve is independent of loading type and magnitude. Hence, the allowable load for beams, such as those shown in Fig. 4.3, can be determined easily by plotting the applied moment diagram below or just touching the envelope of the design curve. One advantage of the PSC method is that it is based on a clear mechanical model where the effect of other parameters such as end anchorage, additional reinforcement and friction at the support can be incorporated separately in the equations. The use of plastic design for continuous composite slabs is also possible (Bode and Dauwel, 1999, Bode et al., 1996).

A procedure to incorporate the effects of end anchorage, frictional interlock and mechanical interlock for use in the PSC method was proposed by Calixto et al. (1998). They suggested plotting test data using $\frac{V_{ut}}{b(L_s + L_o)}$ for the x-axis and $\tau_u = \frac{\eta N_{cf}}{b(L_s + L_o)}$ for the y-axis and then obtaining the regression line. The equation is,

$$\frac{\eta N_{cf}}{b(L_s + L_o)} = \tau_{um} + \frac{\mu V_{ut}}{b(L_s + L_o)} \tag{4.19}$$

where,

τ_{um} = mechanical shear bond strength

μ = friction coefficient given by the intercept and the slope of the regression line. This method showed a much better correlation with the test data when compared to the Eurocode's method.

4.6 Proposed method for calculating shear stress from small scale test

In this section, two approaches, namely the work method and the force equilibrium method for calculating shear bond stress history along the shear span and its relation with the end slip, are presented. Because the methods are based on slab bending, they can be applied to both full and small scale bending tests as long as the test are conducted according to the same test procedure. The shear bond-slip relationship is useful for numerical modeling while the maximum shear stress value can be used in other analytical methods, such as the PSC method, for design.

4.6.1 Work method

The principle of the work method used for composite slab analysis was presented by Wright and Evans (1990). They referred to it as the plastic collapse method. In this procedure, the calculation is made for an ultimate condition where the concrete crack has propagated up to the top fiber at the critical section. The shear bond stress value obtained by the plastic collapse method is therefore a single point at the ultimate load condition. An (1993) used the work method for calculating shear bond stress history from block bending tests (Sec. 2.3.8) but without considering the remaining strength of the steel deck. The method to calculate the shear bond stress history, which considers the remaining strength of the steel deck is described here forth.

The method was derived based on the following assumptions;

1) The relative slip is uniform along the shear span as shown by the test results presented in Sec. 3.7.

2) Slip is only dominant at one end while at the non-failing end, slip is small and negligible.

3) Distribution of horizontal shear stress is uniform along the shear span.

4) Small displacement theory is valid.

5) The curvatures of both concrete and steel deck are equal.

6) Due to slip, two neutral axes exist and therefore the steel deck is always taking a fraction of load by bending about its own axis.

7) The work done by the shear bond force can be calculated only after the slip has occurred. Before that the shear force is assumed to increase linearly from zero to the value calculated at the first end slip. For this purpose the first end slip is considered as 0.02 in.

8) Steel deck is assumed to behave elastically up to the maximum load.

Fig. 4.4 shows typical plots of applied load versus slip from bending tests and Fig. 4.5 is the slab in the cracked condition. Consider at any instance during the test after first end slip has taken place, the external work done by the applied load from instant *i-1* to *i* can be written as,

$$\begin{aligned} W_e &= \frac{P_{i-1}}{2}\Delta\delta_{1i} + \frac{\Delta P_i}{4}\Delta\delta_{1i} + \frac{P_{i-1}}{2}\Delta\delta_{2i} + \frac{\Delta P_i}{4}\Delta\delta_{2i} \\ &= \frac{P_{i-1}}{2}\left(\Delta\delta_{1i} + \Delta\delta_{2i}\right) + \frac{\Delta P_i}{4}\left(\Delta\delta_{1i} + \Delta\delta_{2i}\right) \\ &= \left(\frac{P_{i-1}}{2} + \frac{\Delta P_i}{4}\right)\left(\Delta\delta_{1i} + \Delta\delta_{2i}\right) \end{aligned} \tag{4.20}$$

where,

P_{i-1} = total applied load at instant *i-1*

ΔP_i = load increment from instant *i-1* to *i*

$\Delta\delta_{1i}$ and $\Delta\delta_{2i}$ = deflection increment from instant *i-1* to *i* at load position 1 and 2 respectively.

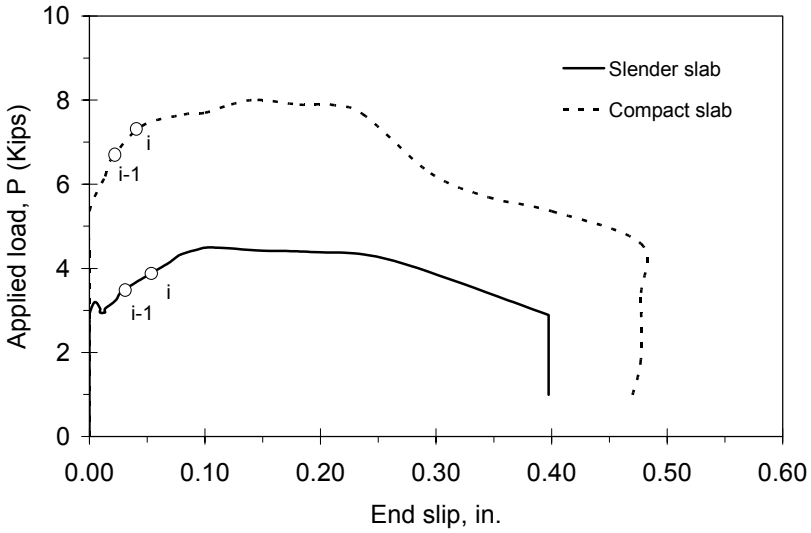

Fig. 4.4 Typical applied load versus end slip for compact and slender slabs

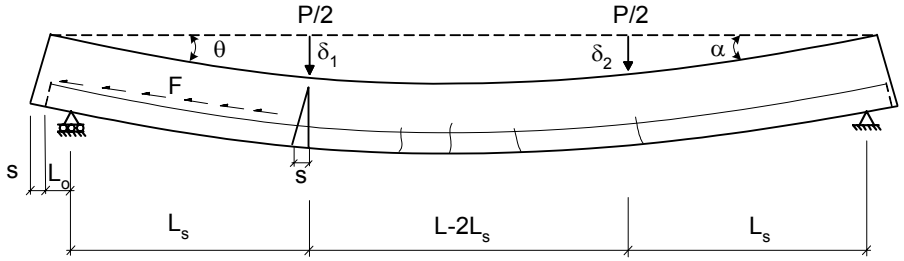

Fig. 4.5 Slab condition at post cracking mode

The internal work that resists the applied load is,

$$W_i = \left(F_{i-1} + \frac{\Delta F_i}{2}\right)(\Delta s_i) + \left(M_{ri-1} + \frac{\Delta M_{ri}}{2}\right)(\Delta\theta_i + \Delta\alpha_i)$$
$$= \left(F_{i-1} + \frac{\Delta F_i}{2}\right)(\Delta s_i) + \left(M_{ri-1} + \frac{\Delta M_{ri}}{2}\right)\left(\frac{\Delta\delta_{1i} + \Delta\delta_{2i}}{L_s}\right) \quad (4.21)$$

where,

F_{i-1} = total shear bond force up to instant *i-1*

ΔF_i = shear force increment from instant *i-1* to *i*

Δs_i = average horizontal slip increment from instant *i-1*to *i*.

$\Delta\theta_i$ and $\Delta\alpha_i$ = slope increment at both ends of the slab. Under small deflection $\Delta\theta_i = \Delta\delta_{1i}/L_s$ and $\Delta\alpha_i = \Delta\delta_{2i}/L_s$ respectively.

M_{ri-1} = moment resistance of the steel deck when horizontal slip has occurred. This moment exists in the partial shear connection mode, where the deck is not only acting as tensile reinforcement for the composite action, but is also able to carry a fraction of load by bending about its own axis.

By equating the external work to the internal work, the shear force term is,

$$F_{i-1} + \frac{\Delta F_i}{2} = \frac{\left(\frac{P_{i-1}}{2} + \frac{\Delta P_i}{4}\right)\left(\Delta\delta_{1i} + \Delta\delta_{2i}\right) - \left(M_{ri-1} + \frac{\Delta M_{ri}}{2}\right)\left(\frac{\Delta\delta_{1i} + \Delta\delta_{2i}}{L_s}\right)}{\Delta s_i} \tag{4.22}$$

Eq. 4.22 can be separated into two parts,

$$F_{i-1} = \left(\frac{P_{i-1}}{2} - \frac{M_{ri-1}}{L_s}\right)\left(\frac{\Delta\delta_{1i} + \Delta\delta_{2i}}{\Delta s_i}\right) \tag{4.23}$$

and,

$$\Delta F_i = 2\left(\frac{\Delta P_i}{4} - \frac{\Delta M_{ri}}{2L_s}\right)\left(\frac{\Delta\delta_{1i} + \Delta\delta_{2i}}{\Delta s_i}\right) \tag{4.24}$$

It must be noted that according to assumption (7) the above equations are applicable only after the horizontal slip has occurred. Before slipping, the slab is in the full interaction mode where the horizontal shear force can be considered to increase linearly up to the first slip whose value is taken as 0.02 in.

Therefore the limit of end slip is,

$$\Delta s_i \geq 0.02 \tag{4.25}$$

From Eq. 4.23 and4.24, the shear bond force at instance *i* can be determined,

$$F_i = F_{i-1} + \Delta F_i \tag{4.26}$$

Because the deck is assumed elastic up to the maximum load, moment can be related to the curvature by,

$$\frac{M}{E_s I_s} = \frac{1}{R} \tag{4.27}$$

where,

I_s = moment of inertia of steel deck

E_s = modulus of elasticity of steel deck

R = radius of curvature

M = bending moment

The above equation is approximate, as full scale test results presented in Sec. 3.8 indicated that yielding did occur in the deck bottom flange before the maximum load was reached.

It can be shown from the geometry of Fig. 4.6 that,

$$\frac{M_{ri-1}}{E_s I_s} = \frac{1}{R_{i-1}} = \frac{\theta_{i-1} + \alpha_{i-1}}{L - 2L_s} \tag{4.28}$$

and,

$$\frac{\Delta M_{ri}}{E_s I_s} = \left(\frac{1}{R_i} - \frac{1}{R_{i-1}} \right) = \frac{\Delta\theta_i + \Delta\alpha_i}{\left(L - 2L_s\right)} \tag{4.29}$$

Substituting $\theta_{i-1} = \frac{\delta_{1i-1}}{L_s}$, $\Delta\theta_i = \frac{\Delta\delta_{1i}}{L_s}$, $\alpha_{i-1} = \frac{\delta_{2i-1}}{L_s}$ and $\Delta\alpha_i = \frac{\Delta\delta_{2i}}{L_s}$ into Eq. 4.28 and Eq.4.29, the bending moment terms of Eq. 4.23 and 4.24 are,

$$M_{ri-1} = \frac{\left(\delta_{1i-1} + \delta_{2i-1}\right)}{L_s\left(L - 2L_s\right)} E_s I_s \tag{4.30}$$

and,

$$\Delta M_{ri} = \frac{\Delta\delta_{1i} + \Delta\delta_{2i}}{L_s\left(L - 2L_s\right)} E_s I_s \tag{4.31}$$

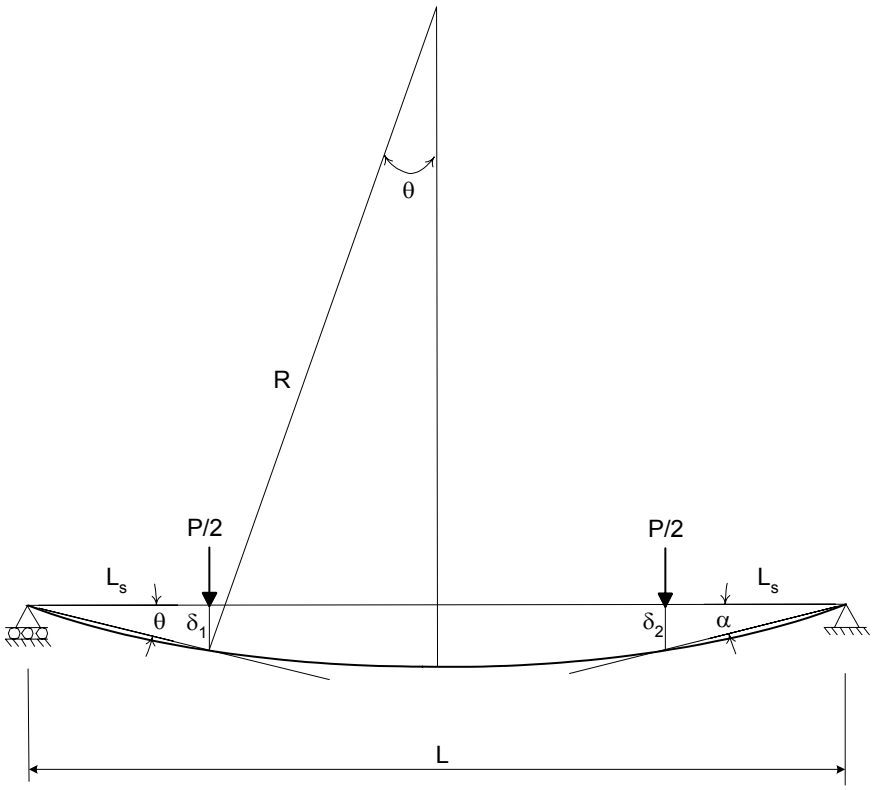

Fig. 4.6 Deflection and curvature of the deck

4.6.2 Force equilibrium method

The force equilibrium method was first introduced by An (1993) to calculate the horizontal shear force-slip relationship for block bending tests. A new derivation of this method is presented here for application to the small scale bending test. In addition to the assumptions listed in the previous section, additional assumptions are made;

1) Plane section remains plane (no shear deformation).

2) Concrete stress in tension is neglected.

3) The neutral axis of the composite section is less than the concrete cover above the deck top flange. Otherwise the neutral axis is considered equal to the concrete depth. This assumption is made based on the observation during the tests that the concrete failed primarily by cracking and the crack tips were always above the deck top flanges.

4) As observed in the test the concrete in compression did not fail by crushing. A major crack was dominant at the critical section where it progressed upward as the end slip increased. The stress-strain behavior of concrete in compression and steel deck in tension is therefore considered linear until the maximum load is obtained.

5) The steel deck section is fully effective.

Fig. 4.7(a) shows the free body diagram of the section of a test specimen at failure, and Fig. 4.7(b) and Fig. 4.7(c) are the corresponding strain and internal force distributions at the critical sections. At any instance during the test, the horizontal shear force F_i is equal to the axial force, T_i in the steel deck which resulted from the composite action. As discussed in the previous section, the steel deck can also take a fraction of the applied load by bending about its own axis. The moment resistance in the steel deck is denoted by M_{ri}. Neglecting the concrete self weight, the shear force, F_i can be calculated by taking moment about the compression force, C;

$$F_i = T_i = \frac{\left(\frac{P_i}{2} L_s - M_{ri}\right)}{z_i} \tag{4.32}$$

where P_i , L_s , and M_{ri} are as defined before, and z_i is the moment arm between tension and compression force.

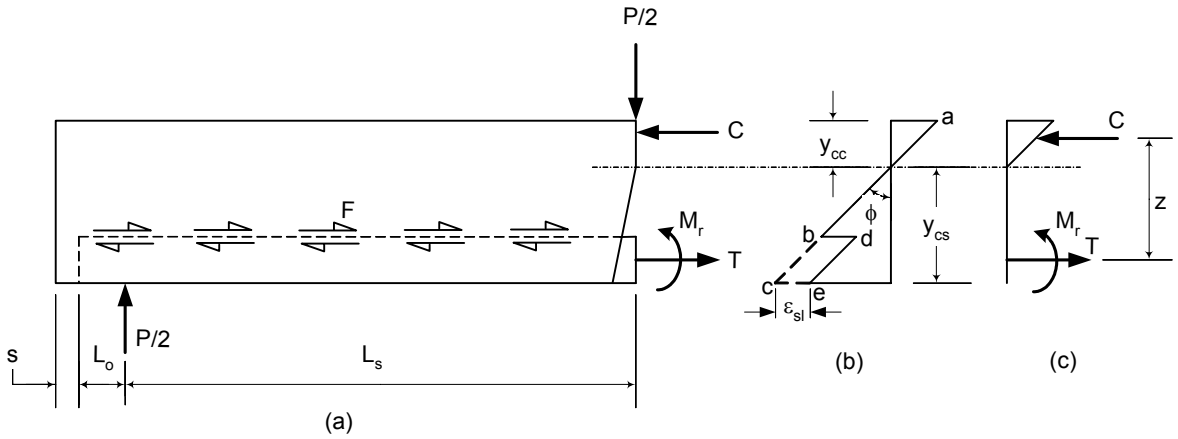

Fig. 4.7 Model for failure section
(a) Free body diagram of the critical section, (b) Strain distribution diagram, (c) Stress diagram

The concrete and the steel deck are assumed to have small vertical separation so that they deflect under the same curvature. Therefore M_{ri} can be determined in a similar manner as in Eq. 4.30;

$$M_{ri} = \frac{\delta_{1i} + \delta_{2i}}{L_s\left(L - 2L_s\right)} E_s I_s \tag{4.30}$$

The moment arm, z_i, is an unknown parameter that is difficult to determine. Its value depends on the location of the composite section neutral axis, which moves upward as the load increases. An approximate location of the composite neutral axis, y_{cc}, is assumed to exist at the first cracking of concrete and then moves upward as the slip and deflection increase. The value off y_{cc} at first cracking is calculated based on a cracked section analysis of full interaction as indicated by line *abc* of Fig. 4.7(b). The calculation can follow Eq. B-1 of ASCE (1992);

$$y_{cc} = d\left\{\left[2\rho n + (\rho n)^2\right]^{\frac{1}{2}} - \rho n\right\} \tag{4.33}$$

where

d = effective depth of deck section

ρ = ratio of steel area to effective concrete area, $\rho = A_s/(bd)$

n = modular ratio = E_s/E_c

Thereafter, y_{cc} moves upwards while the crack length, y_{cs} increases. From geometry, as in Fig. 4.5, the crack length, which depends on the test data, can be estimated by;

$$y_{cs} = \frac{sL_s}{(\delta_1 + \delta_2)} \tag{4.34}$$

Therefore,

$$y_{cc} = d - y_{cs}; \qquad 0 \le y_{cc} \le h_c \tag{4.35}$$

where

h_c = concrete cover depth above deck top flange.

The moment arm is;

$$z = d - \frac{1}{3} y_{cc} \tag{4.36}$$

4.7 Analysis results

Data from the small scale tests was analyzed using the *m-k*, PSC, work and force equilibrium methods as discussed in the previous sections. The analyses were performed following the steps below and the results are presented in the following sub-sections.

1) For the *m-k* method, the coefficients *m* and *k* were obtained in accordance with Eq. 4.1 and 4.2 using data from compact and slender specimens for each deck profile. For the PSC method, the maximum shear bond stress, τ

was evaluated according to the method presented in Sec. 4.5. The shear bond stress history versus end slip was calculated according to the work and force equilibrium methods as explained in Sec. 4.6.1 and 4.6.2.

2) The coefficients were then used to evaluate the theoretical load capacity of slabs whose geometries correspond to full scale configurations. No strength reduction factor was applied in the calculations.

3) The theoretical loads obtained in step 2 were then compared with the maximum loads from full scale tests.

4) The standard deviation of the values obtained in step 3 was determined.

4.7.1 Results of the *m-k* method

The results of analysis according to the ASCE (1992) equation are tabulated in Table 4.1 while the results for the Eurocode 4 (1994) equation are in Table 4.2. The largest difference between the full scale test loads and the calculated loads according to the ASCE equation was 37%. The mean for the ratio of full scale-to-calculated value is 1.04 with the standard deviation 0.16, which indicate that the full scale test results are in good agreement with the calculated values. The same comparisons for the Eurocode 4 equation were 26% for the largest difference, and the mean and standard deviation for the ratio of full scale-to-calculated values are 1.00 and 0.11, respectively. These values suggest that by omitting concrete strength as was prescribed in the Eurocode equation, the spread of results between full scale tests and calculated values can be minimized.

Table 4.1 Results of analysis according to the *m-k* method (ASCE, 1992) and comparison with full scale tests

Specimen ID	Test	*m-k* method from small scale tests						Full scale tests	W_{uf} /W_{um-k}
		X	Y	m	k	f'_{ct} (psi)	W_{um-k} (psf)	W_{uf} (psf)	
3VL20-8-7.5	A	0.0000249	0.809	14568	0.441	3200	1225	1670	1.36
	B	0.0000249	0.797				1225	1650	1.35
3VL20-11-5	A	0.0000193	0.799			5000	456	420	0.92
	B	0.0000193	0.646				456	450	0.99
3VL18-8-7.5	A	0.0000330	0.848	12808	0.450	2900	1339	1790	1.34
	B	0.0000330	0.897				1339	1840	1.37
3VL18-13-5	A	0.0000204	0.705			5000	427	390	0.91
	B	0.0000204	0.717				427	390	0.91
3VL16-4-7.5	A	0.0000970	2.787	24447	0.219	-	-	-	-
	B	0.0000970	2.417				-	-	-
3VL16-8-7.5	A	0.0000441	1.263			3600	2112	2140	1.01
	B	0.0000441	1.303				2112	2230	1.06
3VL16-10-7.5	A	0.0000342	1.023			-	-	-	-
	B	0.0000342	0.902				-	-	-
3VL16-12-5	A	0.0000291	0.993			-	-	-	-
	B	0.0000291	1.000				-	-	-
3VL16-14-5	A	0.0000257	0.859			3300	406	380	0.93
	B	0.0000257	0.891				406	410	1.01
2VL20-7-6.5	A	0.0000267	0.886	31587	0.008	4500	1539	1540	1.00
	B	0.0000267	0.815				1539	1460	0.95
2VL20-9-4	A	0.0000199	0.651			4600	473	460	0.97
	B	0.0000199	0.624				473	480	1.01
2VL18-7-6.5	A	0.0000353	0.996	20605	0.300	2800	1751	1940	1.11
	B	0.0000353	1.060				1751	1790	1.02
2VL18-11-4	A	0.0000223	0.759			4100	430	430	1.00
	B	0.0000223	0.760				430	470	1.09
2VL16-7-6.5	A	0.0000446	1.420	23588	0.308	4500	2474	1860	0.75
	B	0.0000446	1.297				2474	2380	0.96
2VL16-12-4	A	0.0000270	0.919			4300	480	480	1.00
	B	0.0000270	0.969				480	470	0.98
								Mean	1.04
								Standard deviation	0.16

$$X = \frac{V_e}{bd\sqrt{f'_{ct}}}, \qquad Y = \frac{\rho d}{l'_i \sqrt{f'_{ct}}}$$

Table 4.2 Results of analysis according to the *m-k* method (Eurocode 4, 1994) and comparison with full scale tests

Specimen ID	Test	*m-k* method from small scale tests					Full scale tests	W_{uf}/W_{um-k}
		X	Y	m	k	W_{um-k} (psf)	W_{uf} (psf)	
3VL20-8-7.5	A	0.00177	57.50	14568	31.31	1380	1670	1.21
	B	0.00177	56.63			1380	1650	1.20
3VL20-11-5	A	0.00138	56.78			458	420	0.92
	B	0.00138	45.90			458	450	0.98
3VL18-8-7.5	A	0.00234	60.24	14644	27.68	1530	1790	1.17
	B	0.00234	63.72			1530	1840	1.20
3VL18-13-5	A	0.00137	47.28			413	390	0.95
	B	0.00137	48.09			413	390	0.95
3VL16-4-7.5	A	0.00690	198.06	24538	14.87	9448	-	-
	B	0.00690	171.75			9448	-	-
3VL16-8-7.5	A	0.00296	84.75			2162	2140	0.99
	B	0.00296	87.38			2162	2230	1.03
3VL16-10-7.5	A	0.00243	72.73			1384	-	-
	B	0.00243	64.10			1384	-	-
3VL16-12-5	A	0.00207	70.59			563	-	-
	B	0.00207	71.05			563	-	-
3VL16-14-5	A	0.00172	57.60			425	380	0.89
	B	0.00172	59.75			425	410	0.97
2VL20-7-6.5	A	0.00190	62.95	31641	0.43	1540	1540	1.00
	B	0.00190	57.89			1540	1460	0.95
2VL20-9-4	A	0.00134	43.68			473	460	0.97
	B	0.00134	41.87			473	480	1.01
2VL18-7-6.5	A	0.00251	70.76	20605	21.31	1892	1940	1.03
	B	0.00251	75.31			1892	1790	0.95
2VL18-11-4	A	0.00159	53.92			448	430	0.96
	B	0.00159	54.04			448	470	1.05
2VL16-7-6.5	A	0.00317	100.91	24491	19.00	2506	1860	0.74
	B	0.00317	92.20			2506	2380	0.95
2VL16-12-4	A	0.00181	61.62			484	480	0.99
	B	0.00181	65.02			484	470	0.97
							Mean	1.00
							Standard deviation	0.11

$$X = \frac{V}{bd}, \qquad Y = \frac{A_p}{bL_s}$$

4.7.2 Result of the PSC method

Maximum loads from full scale tests and theoretical loads calculated according to the PSC method utilizing small scale data are listed in Table 4.3.

Table 4.3 Results of analysis according to the PSC method and comparison with full scale tests

Specimens ID	Test	PSC method using small scale test data			Max. load from full scale tests, W_{uf} (psf)	W_{uf} / W_{tPSC}
		Max. shear stress, τ_u (psi)	Average, τ_u (psi)	Max. load, W_{tPSC} (psf)		
3VL20-8-7.5	A	30.46	30.10	1280	1670	1.30
	B	29.74		1280	1650	1.29
3VL20-11-5	A	32.02	25.82	475	420	0.88
	B	19.61		475	450	0.95
3VL18-8-7.5	A	29.58	31.05	1420	1790	1.26
	B	32.52		1420	1840	1.30
3VL18-13-5	A	26.22	26.74	420	390	0.93
	B	27.26		420	390	0.93
3VL16-4-7.5	A	86.98	77.33	7350	-	-
	B	67.68		7350	-	-
3VL16-8-7.5	A	43.59	44.74	1980	2140	1.08
	B	45.89		1980	2230	1.13
3VL16-10-7.5	A	39.14	35.34	1270	-	-
	B	31.54		1270	-	-
3VL16-12-5	A	35.34	35.64	627	-	-
	B	35.93		627	-	-
3VL16-14-5	A	28.69	30.10	445	380	0.85
	B	31.51		445	410	0.92
2VL20-7-6.5	A	38.57	36.43	1350	1540	1.14
	B	34.29		1350	1460	1.08
2VL20-9-4	A	23.66	22.66	445	460	1.03
	B	21.66		445	480	1.08
2VL18-7-6.5	A	41.67	43.63	1680	1940	1.15
	B	45.59		1680	1790	1.07
2VL18-11-4	A	34.69	34.77	455	430	0.95
	B	34.85		455	470	1.03
2VL16-7-6.5	A	64.24	60.38	2250	1860	0.83
	B	56.51		2250	2380	1.06
2VL16-12-4	A	41.42	43.85	490	480	0.98
	B	46.28		490	470	0.96
					Mean	1.05
					Standard deviation	0.14

The full scale test results were mostly larger than the calculated values with the ratio of full scale-to-calculated value ranged from 0.83 to 1.31. The mean and the standard deviation of the same ratio were 1.05 and 0.14, respectively. The values suggest that the PSC method is comparable with the *m-k* method.

Data from Table 4.1, 4.2 and 4.3 were plotted in Fig. 4.8 to graphically depict the comparison between the three results. It is clear from the graph that most of the data are spread within 20%[4] with the PSC method generally more conservative that the *m-k* method.

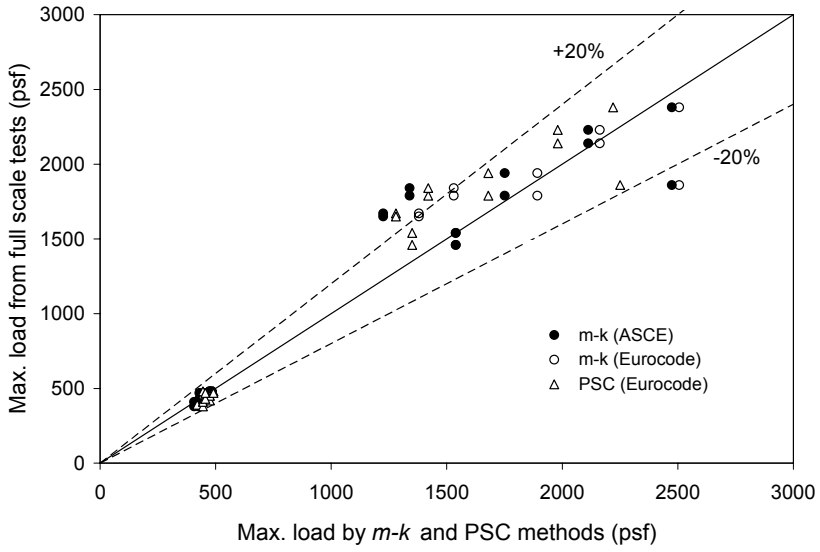

Fig. 4.8 Comparison of results between full scale tests and the *m-k* and PSC methods

Even though the PSC method seems acceptably accurate when compared to full scale tests, its application in design still deserves a comment. The PSC method is only accurate for designing slabs whose geometries are similar to the tested specimens. In the above exercise, the PSC method was applied on each small scale specimen and the calculated values were compared with the full scale specimens of the same geometries.

[4] 20% is, in the author's opinion, a reasonable percentage to indicate a good comparison between two series of data in this study.

Therefore the accuracy is merely depending on the performance of the test specimen and how close the small scale behavior is to the full scale behavior. If the PSC data was compared with the full scale slab of different geometry then the result would not be as accurate. This can be seen by looking at the shear stress values in column 4 of Table 4.3 where the difference of the shear stress values between compact and slender slabs of the same deck are very high. This difference is a source of inaccuracy and lack of flexibility in the PSC method. For example, if one wants to design a slab whose slenderness is different from the slenderness of the tested specimen the result would not be as accurate in that it will be either too conservative for slab that is more compact than the tested specimen or unsafe for slab that is slenderer than the tested specimen. This renders the PSC method suitable only for designing slabs of the same dimension as the tested specimen. A detailed discussion on this inaccuracy and a proposed improvement for the PSC method is given in Sec. 6.5. The same problem is not an issue in the *m-k* method because data from one test group can be used to calculate the capacity of slab of different dimensions and slenderness. This is done through linear interpolation as was laid out in the method.

4.7.3 Result of the work method

The calculation for the work method was done by first plotting the sum of the deflections under line load 1 and 2 against average end slip for all data points beginning from first end slip until the end of the test. Both tests A and B are plotted together as shown in Fig. 4.9(a) and Fig. 4.9(b). As depicted by the graphs, vertical deflections are linearly related to the end slips. Generally, data from compact slabs exhibited less scatter than the data from slender slabs.

Linear regression analysis was then performed on the data and the slope of the line was substituted as a constant value into the $\frac{\Delta\delta_{1i} + \Delta\delta_{2i}}{\Delta s_i}$ terms in Eq. 4.23 and Eq. 4.24. Horizontal shear stress was calculated by dividing the total shear bond force obtained from Eq. 4.26 by the surface area of the steel deck along the shear span. Typical results of shear bond stresses versus end slips are shown in Fig. 4.10. Results of other tests are compiled in Appendix D.

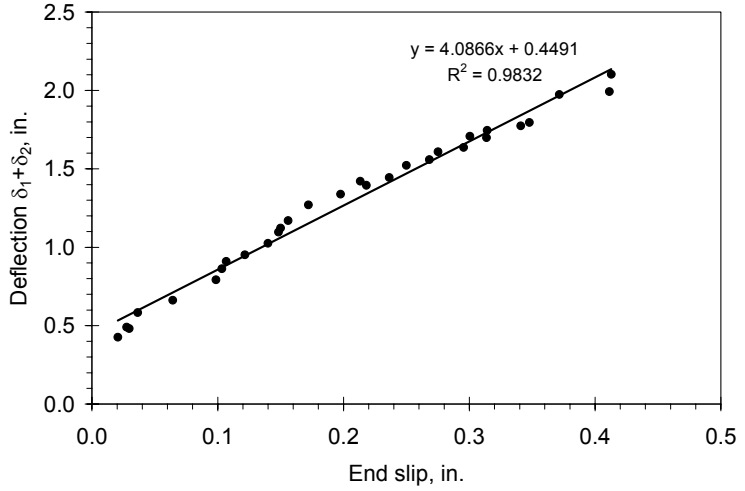

(a)

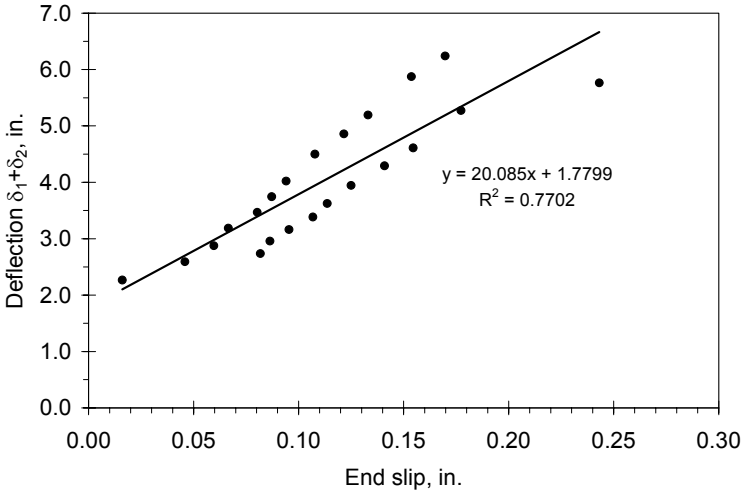

(b)

Fig. 4.9 Total deflection at points 1 and 2 versus end slip
(a) 3VL16-8-7.5s (compact), (b) 3VL16-14-5s (slender)

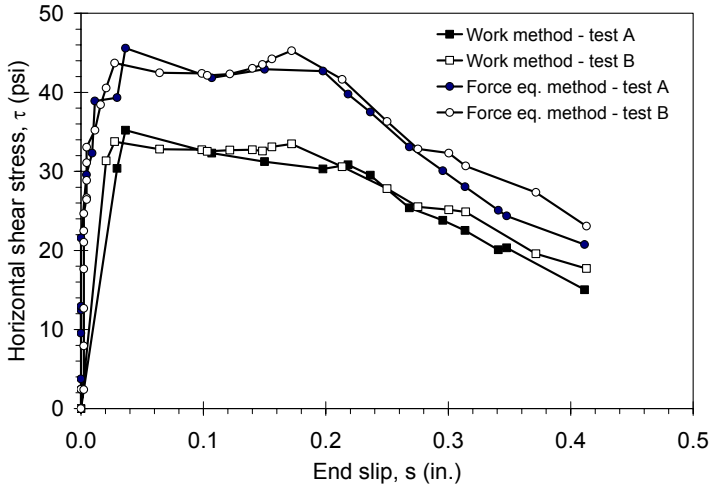

Fig. 4.10 Horizontal shear stress versus end slip for 3VL16-8-7.5s obtained by work method and force equilibrium methods

4.7.4 Result of the force equilibrium method

Each test data point was used in Eq. 4.32 through 4.36. Typical graphs of shear bond stress versus end slip are shown in Fig. 4.10 together with the results of the work method. Generally the shear stresses obtained by the work method are lower than those obtained by the force equilibrium method. The difference was larger for compact slabs than for slender slabs.

4.7.5 Comparison of the PSC with the work and force equilibrium methods

Maximum shear bond stresses obtained from the PSC method (Sec. 4.7.2) and work and force equilibrium methods are listed in Table 4.4. The data is compared graphically in Fig. 4.11. The results show that the work method results are dispersed more widely from the PSC method with the standard deviation of the ratio of PSC-to-work method of 0.28 as compared to 0.12 for the force equilibrium method.

Table 4.4 Maximum shear bond stress from the PSC, work and force equilibrium methods

Specimen ID	Test	Maximum shear bond stress, τ_u (psi)			PSC/WM	PSC/FM
		PSC	Work method (WM)	Force equil. Method (FM)		
3VL20-8-7.5	A	30.46	24.85	31.06	1.23	0.98
	B	29.74	25.84	32.29	1.15	0.92
3VL20-11-5	A	32.02	19.71	25.81	1.62	1.24
	B	19.61	16.84	20.94	1.16	0.94
3VL18-8-7.5	A	29.58	26.36	34.20	1.12	0.86
	B	32.52	28.00	36.33	1.16	0.90
3VL18-13-5	A	26.22	19.92	22.82	1.32	1.15
	B	27.26	17.91	22.46	1.52	1.21
3VL16-4-7.5	A	86.98	66.64	86.60	1.31	1.00
	B	67.68	54.60	70.00	1.24	0.97
3VL16-8-7.5	A	43.59	35.22	45.59	1.24	0.96
	B	45.89	33.76	45.27	1.36	1.01
3VL16-10-7.5	A	39.14	27.29	41.80	1.43	0.94
	B	31.54	22.42	34.10	1.41	0.92
3VL16-12-5	A	35.34	26.87	33.10	1.32	1.07
	B	35.93	25.76	31.70	1.39	1.13
3VL16-14-5	A	28.69	28.87	25.80	0.99	1.11
	B	31.51	29.21	26.80	1.08	1.18
2VL20-7-6.5	A	38.57	23.62	42.68	1.63	0.90
	B	34.29	21.87	39.51	1.57	0.87
2VL20-9-4	A	23.66	21.54	20.45	1.10	1.16
	B	21.66	20.00	21.89	1.08	0.99
2VL18-7-6.5	A	41.67	22.03	44.55	1.89	0.94
	B	45.59	24.40	51.14	1.87	0.89
2VL18-11-4	A	34.69	42.31	30.83	0.82	1.13
	B	34.85	48.72	38.20	0.72	0.91
2VL16-7-6.5	A	64.24	67.51	67.98	0.95	0.94
	B	56.51	62.57	63.00	0.90	0.90
2VL16-12-4	A	41.42	38.20	35.25	1.08	1.18
	B	46.28	41.50	38.26	1.12	1.21
				Mean	1.26	1.02
				Standard deviation	0.28	0.12

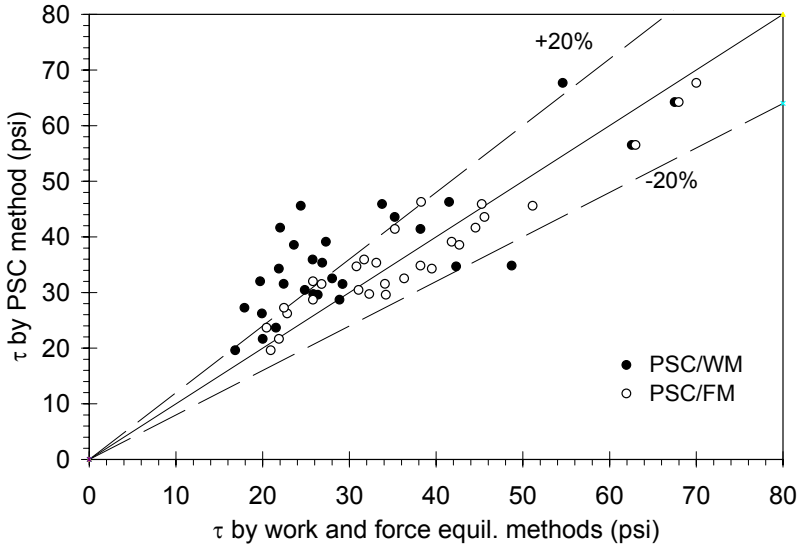

Fig. 4.11 Maximum shear bond stress from PSC, work and force equilibrium methods

Most results from the work method were too conservative with the largest different between the PSC and the work method as high as 89%. There were also unconservative results from the work method with the maximum difference of 28%. On the other hand, results of force equilibrium method showed a better correlation with the PSC method where the difference was less than 14% for the unconservative results and not more than 24% for the conservative results.

The reason for wide dispersion of the work method is that it is too dependent on the test data, especially the end slip. The magnitude of end slip was not consistent between tests of similar configurations. One test might have larger end slip than the companion specimen. The inconsistency of end slip magnitudes influenced the slope of regression line as shown in Fig. 4.9, where the values can become either too large or too small. This would result in incorrect magnification of the shear bond force, which is calculated according to Eq. 4.23 and Eq. 4.24.

4.8 Concluding remarks

1) Application of small scale test data in the *m-k* and the PSC methods was able to predict the capacity of the compatible full scale specimen within acceptable accuracy.

2) The *m-k* method using the Eurocode 4 equation produced more consistent results than the ASCE equation.

3) The *m-k* method produced more accurate and less dispersed results but less conservative results than the PSC method.

4) Both the work and force equilibrium methods can be used for calculating the shear bond stress-slip history from a bending test. In addition to this, the maximum shear bond stress value obtained from this calculation also can be used in other design methods that need the value such as the PSC method. The force equilibrium method demonstrated good correlation with the PSC method while the work method was too conservative.

5) Results in Table 4.4 suggest that the shear bond stress changed with the slenderness where compact slabs possessed larger ultimate shear bond than the slender slabs.